EARTH SURFACE PROCESSES AND LANDFORMS
Earth Surf. Process. Landforms (2009)

Published online in Wiley InterScience
(www.interscience.wiley.com) DOI: 10.1002/esp.1764

Weathering the escarpment: chemical and physical rates and processes, south-eastern Australia

Benjamin C. Burke,[1]* Arjun M. Heimsath,[2] Jean L. Dixon,[2] John Chappell[3] and Kyungsoo Yoo[4]
[1] ExxonMobil Development Company, Houston, TX, USA
[2] School of Earth and Space Exploration, Arizona State University, Tempe, AZ, USA
[3] Research School of Earth Sciences, Australian National University, Canberra, ACT, Australia
[4] Plant and Soil Sciences Department, University of Delaware, Newark, DE, USA

Received 20 June 2007; Revised 25 September 2008; Accepted 29 September 2008

* Correspondence to: Benjamin C. Burke, ExxonMobil, PO Box 4778, Houston, TX 77210, USA. E-mail: bburke@alum.dartmouth.org

ESPL
Earth Surface Processes and Landforms

ABSTRACT: Differences in chemical weathering extent and character are expected to exist across topographic escarpments due to spatial gradients of climatic and/or tectonic forcing. The passive margin escarpment of south-eastern Australia has a debated but generally accepted model of propagation in which it retreated (within 40 Ma) to near its current position following rifting between Australia and New Zealand 85–100 Ma before present. We focus on this escarpment to quantify chemical weathering rates and processes and how they may provide insight into scarp evolution and retreat. We compare chemical weathering extents and rates above and below the escarpment using a mass balance approach coupling major and trace element analyses with previous measurements of denudation rates using cosmogenic nuclides (^{10}Be and ^{26}Al). We find a slight gradient in saprolite chemical weathering rate as a percentage of total weathering rate across the escarpment. The lowlands area, encompassing the region extending from the base of the escarpment to the coast, experiences a greater extent of chemical weathering than the highland region above the escarpment. Percents of denudation attributable to saprolite weathering average 57 ± 6% and 47 ± 7% at low and high sites respectively. Furthermore, the chemical index of alteration (CIA), a ratio of immobile to mobile oxides in granitic material that increases with weathering extent, have corresponding average values of 73·7 ± 3·9 and 65·5 ± 3·4, indicating lower extents of weathering above the escarpment. Finally, we quantify variations in the rates and extent of chemical weathering at the hillslope scale across the escarpment to suggest new insight into how climate differences and hillslope topography help drive landscape evolution, potentially overprinting longer term tectonic forcing. Copyright © 2009 John Wiley & Sons, Ltd.

KEYWORDS: passive margin; soil production; saprolite; chemical weathering; Zr

Introduction

Interdisciplinary studies of passive margin escarpments have furthered our understanding of landscape evolution in response to tectonic forcing. Landscape development in the wake of escarpment retreat may also be attributed to altered climate regimes, including altered mean temperatures and precipitation rates, and the seasonal effects of climate, most importantly altered vegetation types. As a topographic escarpment propagates inland from its point of origin, the landscape erodes both horizontally and vertically. Recent studies across the passive margin escarpment of south-eastern Australia (e.g. Persano *et al.*, 2002; Heimsath *et al.*, 2006) quantify rates of escarpment retreat and highlight different models explaining modes of propagation. For example, Persano *et al.* (2002) used low temperature thermochronometry to support the suggestion (e.g. van der Beek *et al.*, 1999) that the escarpment propagated relatively quickly to its current position following initial escarpment creation. Heimsath *et al.* (2006) used *in situ* produced cosmogenic nuclides (^{10}Be and ^{26}Al) to quantify erosion rates across the escarpment and showed how total denudation rates varied across the landscape.

Because chemical weathering directly impacts landscape evolution rates and processes, the coupling between escarpment propagation and weathering is an essential link in understanding both climatic and tectonic forcing of landscape evolution. Here we quantify chemical weathering rates and signatures across the passive margin escarpment of south-eastern Australia to interpret how climatic differences help drive differences in hillslope processes. Specifically, we examine weathering signatures across the weathered bedrock profile, also known as the saprolite profile, from the soil–saprolite interface to the saprolite–bedrock interface. We expand upon how quantification of saprolite chemical weathering relates to escarpment presence and propagation rates, as well as landscape morphology, later.

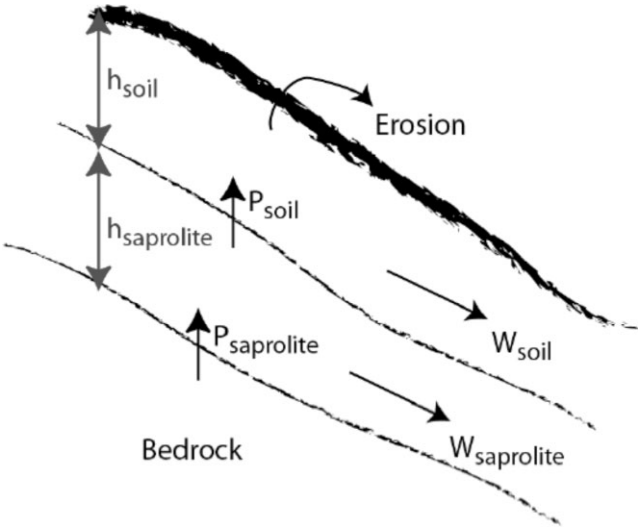

Figure 1. Schematic representation of the weathering mass transfers from bedrock and saprolite to soil. Mass balances in the soil drive the soil thickness, h_{soil}, and are from soil production, P_{soil}, chemical weathering losses, W_{soil}, and physical erosion. Saprolite thickness, $h_{saprolite}$, is governed by rock weathering, $P_{saprolite}$, chemical weathering of the saprolite, $W_{saprolite}$, and soil production.

Weathering at the soil–saprolite interface

Soil, the mobile material that mantles much of the earth, is composed of decomposed organic and inorganic sediments and forms from the actions of both chemical and physical weathering at the soil–saprolite interface (Figure 1). Chemical weathering results in the reduction of bedrock coherence through the weakening of mineral grain boundaries and the increased friability of clays and other secondary weathering products (Kim and Park, 2003). Reduced coherence in saprolite can increase rates of physical weathering, the mechanical processes that produce soil. Relationships between physical and chemical weathering therefore help illuminate the processes shaping hillslope form and its evolution over time (Anderson *et al.*, 2002; Riebe *et al.*, 2003a; Riebe *et al.*, 2001; Stallard and Edmond, 1983). Several such studies also suggest that physical weathering processes likely control chemical weathering processes.

One end member of total weathering processes is in the soil column, where processes of soil production go to completion. Landscapes where the mass balance of the mobile soil column depends on soil production and erosion can be quantitatively characterized as either weathering- or transport-limited (Carson and Kirkby, 1972). When erosion exceeds soil production under equilibrium conditions, bedrock is exposed and erosion is weathering-limited. When soil production is greater than erosion, soils will thicken resulting in a transport-limited landscape. A dynamic balance where soil production balances erosion results in steady-state local soil depth (Carson and Kirkby, 1972; Dietrich *et al.*, 1995; Heimsath *et al.*, 1997). Previous work shows soil production rates decline with increasing overlying soil thickness (e.g. Heimsath *et al.*, 1997, 2000). This negative feedback between erosion and soil production maintains local steady-state soil thicknesses. Soil production rates measured at the top of saprolite using cosmogenic nuclides decrease with soil thickness for all sites across the escarpment, resulting in a consistent soil production function despite different precipitation rates across the study area (Heimsath *et al.*, 2006). In this paper we use major and trace element analyses from saprolite at the base of the soil column to quantify chemical weathering rates and processes at similar locations to those used by Heimsath *et al.* (2006). We also examine the influence of chemical weathering on saprolite column chemistry and at the saprolite–bedrock interface, as described in the next section.

Deep saprolite weathering

Chemical weathering in the saprolite has been investigated at a variety of scales in diverse climates (e.g. Pavich and Obermeier, 1989; Turner *et al.*, 2003; White *et al.*, 1996; White *et al.*, 1998). Geochemical data from borings through the saprolite column at Panola, Georgia and Rio Icacos, Puerto Rico, used major element concentrations to show subtle gradients of chemical weathering between the surface and base of saprolite (White, 2002). Variation in major elements were gradual except at or near the saprolite–bedrock interface, suggesting most chemical weathering in the saprolite occurs at the weathering front. The transformation of crystalline bedrock likely occurs relatively quickly at the base of the saprolite column (Cleaves, 1974, 1993). Indeed, in studies of the saprolite near Washington, DC, Pavich and Obermeier (1989) identified that the active areas of chemical weathering in a saprolite column were at the top and bottom.

In addition to the gradients of chemical weathering extent evidenced from major element concentrations, a consistent gradient may exist in secondary mineral concentrations, the products of chemical weathering, through the saprolite column. One measure of chemical weathering extent through the saprolite column is abrasion pH. At Point Reyes, California, Burke *et al.* (2006) found gradients of two pH units with depth in hand-augered saprolite profiles. Here, we use both bulk chemical and abrasion pH concentrations in borings through saprolite to examine subtle differences in chemical weathering gradients across the escarpment.

Many of the previously referenced saprolite studies focus on the processes of bulk saprolite chemical weathering. Other complimentary studies have examined chemical weathering at the individual mineral grain scale in both natural (Balan *et al.*, 2001; Banfield and Richard, 1989; Taunton *et al.*, 2000a, 2000b; White *et al.*, 1999; White *et al.*, 2001) and laboratory settings (Barker *et al.*, 1998; Hoch *et al.*, 1996; Welch, 2002; Welch and Banfield, 2002; Welch *et al.*, 1999; White *et al.*, 1999). Laboratory studies calculate weathering rates are up to two orders of magnitude faster than those reported by studies done on bulk field samples (White and Brantley, 2003). The studies of microscale weathering and single mineral weathering properties can aid our understanding of bulk weathering processes and can further aid in our interpretation of bulk chemical weathering intensities and rates across the escarpment.

Methods

Quantifying chemical weathering extent

We use the concentrations of major and trace elements from the saprolite collected at the soil–saprolite interface at fieldsites across the escarpment to calculate chemical weathering rates and intensities at each site. Additionally, we calculate chemical weathering extent and mineral depletion for samples collected from saprolite profiles from the soil–saprolite interface to the saprolite–bedrock interface. For each of these samples, the degree of chemical weathering for granitic material can be quantified by applying the Chemical Index of Alteration (CIA) (Kirkwood and Nesbitt, 1991), where all oxide concentrations

DOI: 10.1002/esp

are measured in molar percentages (i.e. the weight percent oxide divided by the molar mass of the oxide):

$$\mathrm{CIA} = \frac{\mathrm{Al_2O_3}}{\mathrm{Al_2O_3} + \mathrm{Na_2O} + \mathrm{K_2O} + \mathrm{CaO}}. \quad (1)$$

This index measures the proportion of a conservative oxide to the sum of major oxides found in granitic bedrock. The CIA value for unweathered granite is unique depending on the particular granite in question, and the unweathered granodiorites of our field areas have CIA values of 60 and 59. Conversely, a highly-weathered soil or saprolite has a CIA of between 90 and 100 (Kirkwood and Nesbitt, 1991; Nesbitt, 1982). Because of the presence of apatite in the parent material and saprolite at our fieldsites, we correct for its affect on CaO using the standard methodology outlined by Price and Velbel (2003, references therein) such that:

$$\text{corrected CaO} = \text{mol CaO} - [(10/3) \times \text{mol } \mathrm{P_2O_5}]. \quad (2)$$

In addition to using the CIA as a relative measure of chemical weathering extent, we use abrasion pH as an absolute measure. As parent minerals, such as biotite and feldspars, in unweathered granite react with groundwater to dissolve and precipitate as secondary minerals, the pH of the saprolite decreases (Grant, 1969). Saprolites and soils become more acidic over time in temperate climates as hydrolysis and solution reactions increase the number of hydrogen ions adhering to mineral boundaries and clay mineral interlayers. Grant (1969) found that the pH of a slurry of hand-abraded saprolite and distilled water decreased as the weathering extent as measured by percentage of clay minerals in the saprolite increased. Because of the strong correlation between percent of clay minerals and abrasion pH, we use this method as an absolute measure of chemical weathering extent in saprolite.

Calculating the chemical weathering rate

We follow the same geochemical mass balance method as used in Burke *et al.* (2007). This method is similar to Brimhall *et al.* (1991, 1992) and described by Riebe *et al.* (2001, 2003a, 2003, b) to calculate bulk chemical weathering rates. The soil production rate (P_{soil}), determined by *in situ* cosmogenic nuclide concentrations measured at the top of the saprolite column is equal to the landscape denudation rate (D) (Heimsath *et al.*, 1997). The landscape denudation rate is equal to the sum of the chemical weathering rate (W) and the physical erosion rate (E) such that,

$$P_{soil} = D = E + W \quad (3)$$

The saprolite chemical weathering rate is a function of denudation using enrichment of immobile element, such as zirconium, in saprolite compared to its unweathered parent material, following methods of Riebe *et al.* (2003a):

$$\mathrm{CDF}_{saprolite} = \left(1 - \frac{[\mathrm{Zr}]_{rock}}{[\mathrm{Zr}]_{saprolite}}\right) \times 100. \quad (4)$$

The CDF represents the percentage of total denudation accounted for by chemical weathering, and the weathering rate of saprolite is then calculated as:

$$W = D\left(1 - \frac{[\mathrm{Zr}]_{rock}}{[\mathrm{Zr}]_{saprolite}}\right) \quad (5)$$

Calculating volumetric strain and elemental change

To examine the variations and effects of chemical weathering through the saprolite column, we calculate the quantitative gains or losses of an element relative to the unweathered parent material at the base of cores drilled through the saprolite to the saprolite–bedrock boundary. This quantitative method was developed by Brimhall and Dietrich (1987) and has been used by several recent studies (Brimhall *et al.*, 1991; Chadwick *et al.*, 1990; White *et al.*, 1996; White *et al.*, 2001). The gains or losses of an element j are determined by the ratio of the concentration of the weathered component, $C_{j,w}$ to that of the unweathered parent material, $C_{j,p}$ such that:

$$\frac{C_{j,w}}{C_{j,p}} = \frac{\rho_p}{\rho_w}\frac{1}{(\varepsilon_i + 1)}(1 + \tau_j), \quad (6)$$

where the ratio of density change, ρ_p/ρ_w, is associated with the dissolution and precipitation of mobile elements. The strain factor, $1/(\varepsilon_i + 1)$, represents the volume ratio of the weathered material to the parent, V_w/V_p, resulting from soil compaction or extension where $\varepsilon_i = V_w/V_p - 1$. Volume and density changes together describe closed system contributions without regard for movement of the element in question. The mass transport coefficient τ_j is an open-system contribution that describes the mobility of element j within a unit volume of saprolite (Brimhall *et al.*, 1991; White *et al.*, 1996).

Volumetric strain (change), ε_i, is calculated as the ratio of the products of densities and concentrations of an immobile element in the saprolite and parent material as:

$$\varepsilon_i = \frac{\rho_p C_{i,p}}{\rho_w C_{i,w}} - 1. \quad (7)$$

Positive values of ε_i indicate saprolite expansion and negative values indicate volume loss. Values of ε_i around zero indicate isovolumetric weathering.

Elemental loss or gain during weathering is characterized by the mass transfer coefficient τ_j. It is computed from density and chemical composition data in combination with volume change derived from the strain calculations as:

$$\tau_j = \frac{\rho_w C_{j,w}}{\rho_p C_{j,p}}(\varepsilon_i + 1) - 1 \quad (8)$$

when $\tau_j = -1$, element j has been completely removed by chemical weathering. If $\tau_j = 0$, the element is immobile during weathering. Values of $\tau_j > 0$ indicate mass gain during weathering.

Calculation of the weathering front propagation rate

Isovolumetric weathering in saprolite can be formulated as the rate of downward movement, ω_{sp}, (in m $\mathrm{Ma^{-1}}$) of the bedrock–saprolite interface. It is calculated by dividing the mass flux, Q_w, of solute transported from the weathering profile (in kg $\mathrm{m^{-2}\,s^{-1}}$) by the product of the density of the parent material (2700 kg $\mathrm{m^3}$) and the saprolite porosity, ν_ϕ [estimated from the ratio of density change, ρ_p/ρ_w (Cleaves, 1993)]:

$$\omega_{sp} = \frac{Q_w}{\rho_p}\frac{1}{\nu_\phi} \quad (9)$$

We calculate the mass flux of solute, Q_w, as the product of average annual stream flow from the nearby stream and

DOI: 10.1002/esp

measured solute concentrations from the surface water source at baseflow and the measured solute concentration in rainfall (McDowell and Asbury, 1994). This method allows us to calculate an approximate, catchment-averaged weathering front propagation rate. Given the difficulty of accessing groundwaters or porewaters at the saprolite–bedrock interface and sampling those waters over a longer-term study, this method provides a useful estimate of the weathering front propagation rate from a single sample event without a more detailed installation and sampling program. Furthermore, by sampling rivers at baseflow above and below the escarpment contemporaneously, we can assess the relative differences in weathering rates between the highland and the lowlands. The data to determine the ratio of density change represents the mean of samples collected from each field site. Using porosity data derived from one site to average across a catchment underlines the approximate nature of this calculation, as it assumes lithologic homogeneity throughout the catchment. We address the issue of lithology at each fieldsite later.

We offer this method for approximating the weathering front propagation rate based on stream chemistry data not in spite of, but conscious of, the limitations on the method suggested by Taylor and Velbel (1991), Likens and Bormann (1995), and Pavich (1986) on account of precipitation, vegetation, and temperature fluctuation from seasonality. To account for seasonal variations in precipitation, temperature, and the associated vegetation response to climatic seasonality, Likens and Bormann (1995) suggest that a sampling program over seven years is needed to overcome seasonality and storage effects. Pavich (1986) suggests that the error on short-term weathering rates can be greater than 100% because of the unconstrained differences in discharge measurements between sample locations and time. We acknowledge all those sources of potential error and argue that our limited sampling program constrains all those potential error sources by taking a snapshot of water chemistry at stream-fed baseflow during a season when deciduous plants are dormant in an area underlain by bedrock of similar physical properties.

Sampling and analytical methods

We collected samples from the entire vertical saprolite profile using a diesel-powered rotary drill rig mounted on a heavy-duty truck. We used an HQ-sized (14·53 cm diameter) low-speed dry auger system to advance the hole and a direct-push coring system contained within the drill stem to sample at desired intervals. When we could not advance the HQ system any deeper, we switched to a water-cooled, NQ (7·53 cm diameter) diamond and tungsten high-speed carbide rotary drill system to advance the hole through high-density saprolite and crystalline bedrock. We collected core while drilling into a split-spoon core tube within the drill stem. The core was recovered by wireline without removing the drill bit and drill stem.

Samples of saprolite were analyzed using a Rigaku X-ray fluorescence (XRF) spectrometer. We prepared fused glass beads to determine major element concentrations (SiO_2, Na_2O, CaO, Al_2O_3, and K_2O). Trace elements were determined from pressed pellets (Zr, Ce, and Th). Each sample was homogenized; a 20 g subsample of each was dried at 110 °C for 24 hours. Following powdering in a tungsten carbide mill, the samples were ashed at 920 °C for 12 hours to calculate loss-on-ignition (LOI) values. The discs for major element analysis were fused from a homogenized powder containing 0·7 g of sample and 7 g of equal proportions of lithium metaborate and lithium tetraborate. The pellets for trace elemental determination were pressed from a homogenized powder containing 7 g of sample and 3·5 g of lithium borate binder.

We measured abrasion pH on all samples using equal proportions of saprolite and distilled water. The sample and water slurry sat for 20 min prior to measurement by a glass membrane pH electrode. The calibration of the pH electrode was checked at the beginning and end of each data collection period.

Water samples from the Nunnock River near the fieldsite and from the Bredbo River at Frog's Hollow were collected during the same week in sterile, acidified bottles to calculate the approximate weathering front propagation rate (Equation 9). In the laboratory, the samples were filtered to remove particulates prior to cation analysis by inductively-coupled plasma mass spectroscopy (ICP-MS). It is important to note that both samples were collected at baseflow conditions from actively flowing rivers during a week in which no precipitation occurred. Both highland and lowland sites were experiencing a drought and little precipitation had fallen in the months preceding the sampling. We assume these samples represent present cation flux from the watershed because of the fluvial base flow conditions and are considered valid for use in approximating a catchment-averaged saprolite weathering front propagation rate (Cleaves, 1993). While a greater number of samples would constrain the error associated with discharge measurement, our two samples, collected contemporaneously, allow us to examine the relative differences between the sites. Given the baseflow conditions of the river, and our assumption that the cation flux at baseflow represents an average value from the catchment, we estimate that the bulk of the uncertainty in this measurement is analytical uncertainty.

Study Sites

The seaward-facing escarpment inland of the south-eastern coast of Australia is the ideal natural laboratory for this study of deep saprolite weathering across an escarpment (Figure 2). The Australian passive margin escarpment is similar in shape and topography to others across the world (Matmon *et al.*, 2002). Much of the work that has gone into quantifying processes across this escarpment has focused on either long-term denudation rates or escarpment evolution and propagation. This escarpment, and indeed the continental margin of south-eastern Australia, was likely formed as a result of rifting between Australia and the Lord Howe Rise during the mid-Cretaceous (85–100 Ma) (Hayes and Ringis, 1973; Weissel and Hayes, 1977). Results from apatite fission-track thermochronometry suggest that the escarpment propagated quickly to near its present location between 35–50 Ma in the early to mid-Cenozoic and has been roughly stable since then (Cockburn *et al.*, 2000; Matmon *et al.*, 2002; O'Sullivan *et al.*, 1996; Persano *et al.*, 2002). The method of escarpment propagation was likely a rollback mechanism in which headward watershed erosion provided the forward movement. A small unroofing component of erosion may have removed material from the highlands at and above the escarpment (Persano *et al.*, 2002). When escarpment propagation ceased, a contrast in exposure histories across the escarpment existed. Therefore, given the similar denudation histories of fieldsites across the escarpment (Heimsath *et al.*, 2006), saprolite columns should vary in weathering extent as well as thickness.

The soil production rates at the fieldsites across the escarpment are similar (Heimsath *et al.*, 2006) despite different precipitation regimes, average annual temperatures, and placement relative to the escarpment, suggesting that soil production processes are similar. At all three sites, small

DOI: 10.1002/esp

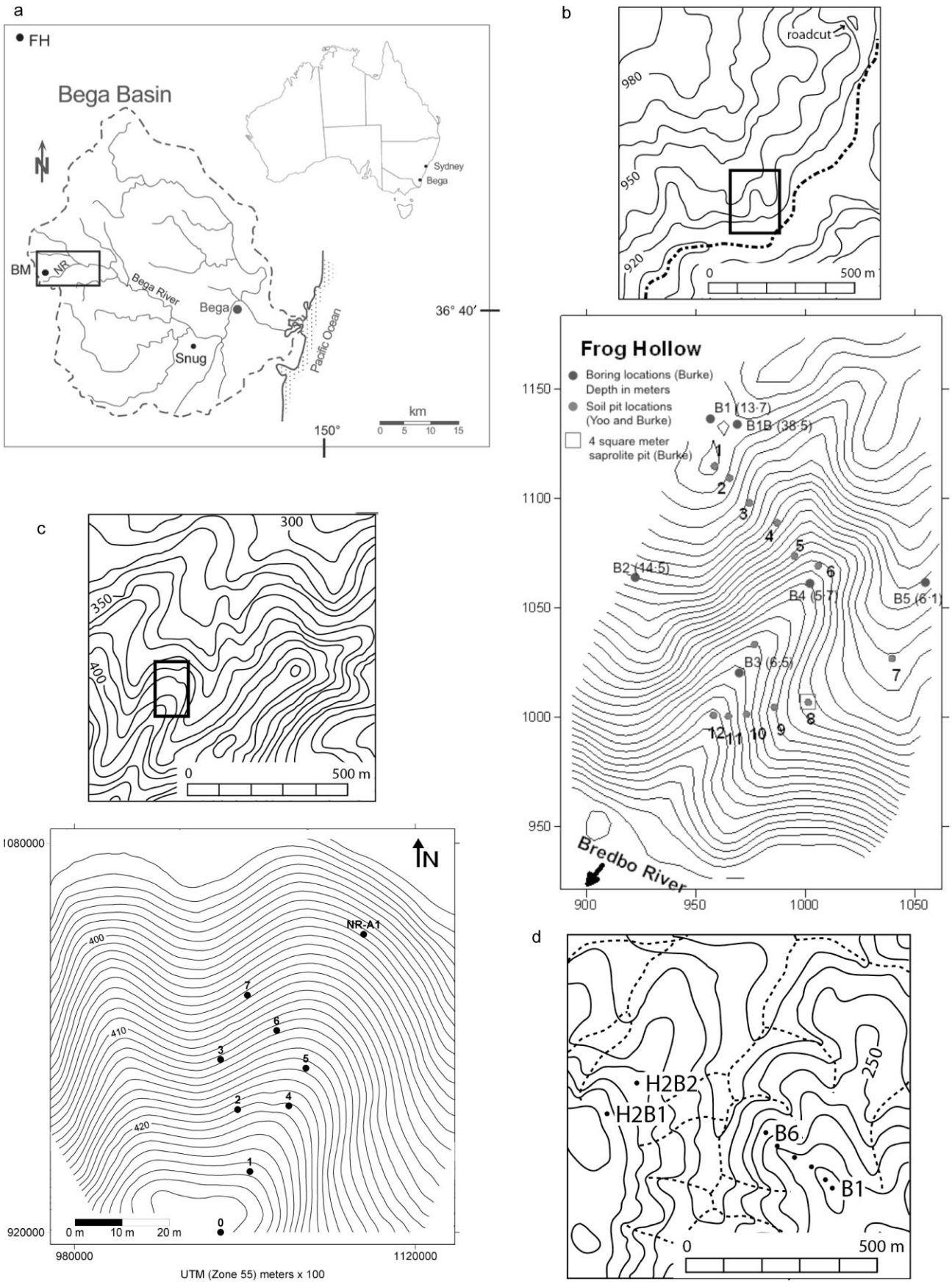

Figure 2. (a) The regional map for the three fieldsites. The Frog's Hollow (FH) site is 30 km north of Nunnock River (NR) above the escarpment. The rectangle around NR is the escarpment face (Heimsath *et al.*, 2000, 2006). The Snugburra, abbreviated as Snug (SN) site is near the town of Bemboka, New South Wales, 15 km south-east of NR. (b) The local map and site map for FH. The FH local map shows the Bredbo River as a dashed line. The site map shows the location of the numbered soil pits. Boring locations are also shown. In parenthesis, the depths of the borings are indicated in meters adjacent to the borings. The location of a 2 m pit used for another study is shown by a square at soil pit 8. Elevations are shown in meters. Contour interval on the site map is 1 m. (c) The local map and site map for NR. The fieldsite is located inside the rectangle on the local map. The site map shows the location of the numbered soil pits. The boring location is at NR-A1. Elevations are in meters. (d) The local map for SN. Watercourses are shown as dashed lines. The site map shows the location of the numbered soil pits, B1–B6. The boring locations are H2B1 and H2B2. Elevations in meters.

DOI: 10.1002/esp

mammals are responsible for bioturbation and soil mass movement. Wombats, echidnas, and lyrebirds are the primary mammalian and avian agents of bioturbation and only burrow in the soil column. Insects are also responsible for bioturbation. We have also observed anthills, some over a meter in height.

We used three different fieldsites for this study. Two were first described by Heimsath *et al.* (1999, 2000, 2006), and used subsequently for further studies (Heimsath *et al.*, 2002, 2005, 2006; Green *et al.*, 2006; Yoo *et al.*, 2006) (Figures 2b–2c). The highland site [Frog's Hollow (FH), Figure 2b] is 12 km inland of the escarpment on the low-relief Monaro plain near Bredbo, New South Wales. At approximately 950 m above sea level, the site receives 600–700 mm of precipitation annually (Australia B.o.M., 2003). Some of that precipitation has been observed in this study and others to fall as sleet and snow and some freeze-thaw processes occur at the site (Heimsath *et al.*, 2001). The highlands, as measured over 76 years from the town of Nimmitabel, approximately 15 km to the south at a similar elevation, have an annual maximum temperature of 15·6 ± 5·6 °C (mean ± monthly standard deviation) and a minimum of 3·4 ± 3·9 °C with three months having a mean minimum temperature below 0 °C and two additional months with mean minimum temperatures less than 1 °C (Australia B.o.M., 2003). Indeed, the site is likely to have experienced Pleistocene periglacial effects from nearby glaciers in the Snowy Mountains (Galloway, 1965). The low relief, open grasslands and savanna forest around the highlands site are currently used for sheep grazing and ranching. The site is underlain by the Anembo granodiorite, part of the Mesozoic-aged Jerangle igneous complex (Richardson, 1976).

The first of two lowland sites, the Nunnock River (NR) site, is at the base of the escarpment, 60 km to the south-east of the highland site (Figure 2c). At approximately 450 m above sea level, below the headwaters of the river by the same name, the site receives 1100 mm of rain annually (Australia B.o.M., 2003). The site is not likely to have experienced Pleistocene periglacial effects and currently it rarely receives frozen precipitation. The coastal lowlands, as measured over 56 years from the town of Bega, approximately 30 km to the east, have an annual maximum temperature of 22·2 ± 3·8 °C (mean ± monthly standard deviation) and a minimum of 8·3 + 4·7 °C with no months having a mean minimum temperature below 0 °C (Australia B.o.M., 2003). Vegetation changes since the Pleistocene have been minimal (Galloway, 1965). Several eucalyptus species forest the site with little understory. The underlying bedrock is the Bemboka granodiorite, a member of the suite of crystalline rocks comprising the Bemboka batholith. Lewis *et al.* (1994) describes the granodiorite as very mineralogically homogenous.

The second of the two lowland fieldsites, Snugburra, abbreviated as Snug (SN), is seaward 15 km from the Nunnock River lowland site (Figure 2d). At approximately 200 m above sea level, it is on a low-relief coastal plain dotted with dairy farms, but has no record of intense land use or tillage agriculture. With its proximity to the base of the escarpment at Nunnock River, it is assumed to have similar rainfall and temperature. It is also underlain by the Bemboka granodiorite.

We note that all three sites are underlain by granodiorites, the Anembo granodiorite at the highlands site and the Bemboka granodiorite at the lowlands sites. Table I notes the bulk major and trace geochemistry of the two unweathered granitoids. Although we note variability between the two formations in the base cations and Zr concentrations, we note that the unweathered material yields almost identical CIA values above and at the base of the escarpment, 59·4 and 59·9 respectively. Additionally, different minimum unweathered Zr concentrations at the three sites yield proportionally similar chemical depletion factors across the escarpment from samples that have experienced conservative enrichment during chemical weathering.

Results and Discussion

We present the major and trace element data from the unweathered rock samples from all three sites in Table I. Data from saprolite pits collected from the highland and lowland sites are presented in Tables II and III. Tables IV–VI present data collected from saprolite borings at all three sites. Data tables include pH data and CIA values for all data points. We also present the major cation concentrations present in baseflow riverwater and precipitation from the highland and base-of-the-escarpment lowlands fieldsites in Table VII. In this section, we examine the elemental concentrations, CIA values, pH trends, volumetric change, and elemental change for each saprolite pit and boring at each site. We then interpret the relationships seen in the data in light of chemical weathering processes, climate, and position relative to the escarpment.

Chemical and physical weathering at the soil–saprolite interface across the escarpment

We collected saprolite samples from the top of the saprolite column in a total of 34 soil pits and borings from three fieldsites across the escarpment (Figures 2b–2d). Using major oxide concentrations and Equation 1, we calculated chemical weathering intensities via the CIA. We calculated saprolite chemical weathering rates using Equation 5 and measured Zr concentrations from the saprolite surface in each soil pit and at the top-of-boring data point from the saprolite cores, Plotting those chemical weathering rates with soil production rates determined by Heimsath *et al.* (2006) shows that the

Table I. Major and trace element data from the unweathered rock samples from all three sites

Pit	Soil column thickness (cm)	Bulk density (g cm^{-3})	SiO_2 (%)	Al_2O_3 (%)	CaO (%)	Na_2O (%)	K_2O (%)	P_2O_5 (%)	Zr (ppm)	CIA[e]
FH parent[a]	–	2·65	68·4	14·8	4·0	2·8	2·9	0·1	84[d]	65·2
NR parent[b]	–	2·65	71·7	13·6	2·9	2·7	3·5	0·1	87[d]	62·0
SN parent[c]	–	2·65	56·1	19·3	0·6	7·5	0·2	0·1	87[d]	60·6

[a] Major oxide concentrations taken from tor samples (Chappell and White, 1976).
[b] Major oxide concentrations taken from tor samples (Joplin, 1963).
[c] Major oxide concentrations taken from core sample H2B2-22·2.
[d] Zr concentration from boring.
[e] CIA reported in all tables uses molar percent oxides, while oxides are reported in mass percent.

DOI: 10.1002/esp

Table II. Depth, major, and trace element compositions of pit samples

Pit	Soil column thickness (cm)[a]	Bulk density (g cm^{-3})	SiO_2 (%)	Al_2O_3 (%)	CaO (%)	Na_2O (%)	K_2O (%)	P_2O_5 (%)	Zr (ppm)
FH1	52	1·78	81·5	12·1	0·4	1·2	3·9	0·03	106
FH2	50	1·73	81·5	12·6	0·6	1·1	3·8	0·04	211
FH3	55	1·81	74·6	16·0	1·5	2·2	3·0	0·05	162
FH4	65	1·55	74·6	14·7	1·9	2·5	3·1	0·08	169
FH5	40	–	70·8	12·6	1·8	1·8	3·0	–	232
FH6	104	–	71·4	13·0	1·6	4·0	3·4	–	177
FH7	58	–	75·1	15·4	1·5	2·0	3·2	0·04	173
FH8	65	1·79	73·4	15·7	0·5	3·3	3·4	0·06	160
FH9	48	1·97	74·9	14·9	0·4	3·2	3·4	0·06	157
FH10	55	–	78·1	13·1	0·6	3·3	5·4	0·03	33
FH-B1	50 (96)	–	71·0	14·3	1·6	2·3	3·4	0·06	117
FH-B2	30 (100)	–	70·7	13·9	2·1	2·4	3·2	0·07	140
FH-B3	70 (120)	–	72·6	13·4	1·5	2·0	3·5	0·04	150
FH-B4	70 (120)	–	72·1	13·6	1·6	2·1	3·3	0·03	218
FH-B5	25 (60)	–	66·8	16·7	1·3	1·8	3·6	0·02	131
FH-2MP	35	–	70·5	14·7	0·8	2·3	3·5	0·07	123
NR0	65	1·74	70·9	16·4	1·0	2·2	2·9	0·04	183
NR1	75	1·58	68·5	17·1	1·2	2·6	3·4	0·03	207
NR2	72	1·57	78·5	13·8	0·8	1·5	2·7	0·03	205
NR3	72	1·82	76·6	15·0	0·8	1·9	3·7	0·03	361
NR4	49	1·90	70·0	17·6	0·8	1·8	2·9	0·03	220
NR5	30	1·79	66·4	18·4	1·8	1·8	2·5	0·03	187
NR6	58	1·61	70·9	16·9	1·7	2·1	3·2	0·03	208
NR7	75	1·82	70·0	17·1	2·0	2·2	2·9	0·06	202
NR-A1	60	–	78·7	13·9	0·6	1·5	3·7	0·03	176
NR-2MP	50	–	74·2	12·5	0·8	1·5	3·2	0·03	236
SN-B1	50	–	60·3	18·6	0·5	1·4	2·3	0·03	203
SN-B1B	65	–	60·4	17·7	0·7	1·2	2·2	0·02	160
SN-B2	66	–	60·4	17·7	0·7	1·2	2·2	0·03	133
SN-B3	40	–	64·8	16·6	0·3	1·9	2·4	0·02	179
SN-B4	40	–	62·9	16·5	0·8	1·6	2·4	0·04	139
SN-B5	55	–	59·5	18·5	0·6	1·0	1·8	0·03	174
SN-B6	60	–	75·8	11·8	0·6	1·0	2·8	0·03	334
H2B1	70	–	65·6	15·1	0·6	1·3	2·2	0·02	155
H2B2	60	–	62·5	16·4	0·5	1·9	3·1	0·04	224

[a] Values in parenthesis represent sampling depth.
Note: Bulk density values are means, $n = 3$.

chemical weathering rate of saprolite decreases with increasing overlying soil thickness (Figure 3a) for all sites. It follows that chemical weathering rates vary slightly across the landscape and across the escarpment, given the variation of soil depths observed across the three fieldsites. The direct coupling suggested by Burke *et al.* (2007) between the physical processes producing soil from the underlying saprolite and the chemical weathering rate of saprolite is confirmed at these sites spanning the escarpment by the relationship between chemical and physical weathering rates shown in Figure 3(a). Chemical weathering rates are similar between sites, following the similarity between the soil production functions for all the sites (Heimsath *et al.*, 2006).

Chemical weathering extent as measured by abrasion pH does not vary with soil column thickness (Figure 3b). Differences within the upper saprolite column, however, are apparent even within one fieldsite. Highland samples with pH values between 7 and 8 were collected from the top of machine-drilled borings and are significantly less weathered than samples collected at the soil–saprolite interface despite being collected only between 35 and 60 cm beneath the boundary. The two orders of magnitude difference between pH values collected at the interface and 35 to 60 cm beneath ground surface suggests the importance of vadose zone processes to chemical weathering. Preferential water flow and the associated zones of weathering extent are likely important drivers in creating the observed difference between the pH of samples from the top of saprolite versus those in the saprolite. Preferential flow pathways in saprolite may form as a result of the density variations between strained (volume-collapsed) saprolite and relict crystalline bedrock structure that likely directs water flow along the boundaries of mineral grains, intrusions, and large-scale features.

Plotting the saprolite CDF, or chemical weathering rates as a percentages of total denudation (CWF as % D), against soil column thicknesses (Figure 3c) across all three sites, we show a slight increase in chemical weathering extent with increasing soil column thickness. Data from the highland site (FH) indicate that chemical weathering constitutes a mean of 48% of total weathering, while the lowland sites have higher means, 58% at the base of the escarpment (NR), and 55% at the lowland site towards the coast (SN). The results from the highland site agree well with a previous study finding that chemical weathering accounted for 40% of soil weathering in soils at the same site (Yoo *et al.*, 2007). Although the Yoo *et al.* (2007) study examined chemical weathering in soils and not in saprolite, their results provide insight into chemical weathering in saprolite. With easy availability of meteoric waters and material that is less weathered than that found in soils, chemical weathering of saprolite sets the stage for further weathering in the soil column and may account for a greater percentage of total denudation than it does in soils. The flux of major and

DOI: 10.1002/esp

Table III. Chemical weathering rates and intensities

Sample	Soil column thickness (cm)[a]	Slope (deg)	CWR (m My^{-1})	SPR[b] (m My^{-1})	%*D*	pH	CIA
FH1	52	2	3·9 ± 1·2	18·7 ± 1·0	25 ± 12	5·59	66·1 ± 3·5
FH2	50	14	11·7 ± 0·6	19·5 ± 1·0	62 ± 3	5·63	68·0 ± 3·5
FH3	55	15	8·5 ± 0·7	17·6 ± 1·0	51 ± 5	5·50	69·8 ± 3·6
FH4	65	18	7·3 ± 0·5	14·4 ± 1·0	53 ± 5	5·56	66·1 ± 3·3
FH5	40	16	15·2 ± 0·7	23·8 ± 2·2	66 ± 5	5·63	65·5 ± 3·3
FH6	*104*	*12*	*3·5 ± 0·2*	*6·6 ± 1·0*	*55 ± 7*	*5·79*	*59·0 ± 3·0*
FH7	58	4	8·6 ± 0·6	16·6 ± 1·0	54 ± 4	5·71	69·4 ± 3·5
FH8	65	8	6·9 ± 0·6	14·4 ± 1·0	50 ± 5	5·19	63·2 ± 3·5
FH9	48	12	9·5 ± 0·8	20·3 ± 1·2	49 ± 5	5·45	62·5 ± 3·5
FH10	55	17	0·0[c]	17·6 ± 1·0	1 ± 2[c]	5·92	53·7 ± 2·9
FH-B1	50 (96)	5	5·0 ± 1·1	17·6 ± 1·0	32 ± 10	6·96	65·6 ± 3·2
FH-B2	*30 (100)*	*12*	*11·0 ± 1·41*	*27·4 ± 4·5*	43 ± 10	*7·30*	*65·0 ± 3·1*
FH-B3	*70 (120)*	*6*	*5·0 ± 0·5*	*11·4 ± 1·0*	*47 ± 6*	*7·62*	*65·8 ± 3·2*
FH-B4	*70 (120)*	*8*	*7·0 ± 0·4*	*11·4 ± 1·0*	*63 ± 5*	*7·27*	*65·8 ± 3·2*
FH-B5	25 (60)	9	11·0 ± 1·7	30·6 ± 4·5	39 ± 10	7·45	70·8 ± 3·5
FH-2MP	35	8	7·8 ± 1·5	24·5 ± 5·0	35 ± 13	5·26	65·9 ± 3·4
Highland mean	55	10	8·1 ± 0·8	19·7 ± 1·7	48 ± 7	6·11	65·5 ± 3·3
NR0	65	9	7·6 ± 0·5	14·4 ± 3·0	52 ± 10	5·12	70·7 ± 3·5
NR1	75	11	6·9 ± 0·4	11·8 ± 2·0	58 ± 8	5·22	68·1 ± 4·0
NR2	72	16	7·2 ± 0·2	12·6 ± 2·0	57 ± 8	5·30	71·8 ± 3·7
NR3	*72*	*19*	*9·5 ± 0·4*	*12·6 ± 2·0*	*76 ± 8*	*5·71*	*67·7 ± 3·6*
NR4	49	11	12·0 ± 0·6	19·9 ± 4·0	60 ± 10	5·85	74·2 ± 4·6
NR5	30	13	15·6 ± 1·0	29·1 ± 5·0	53 ± 9	5·32	76·2 ± 4·3
NR6	58	16	9·7 ± 0·5	16·6 ± 2·0	58 ± 6	5·86	70·8 ± 4·4
NR7	*75*	*18*	*6·7 ± 0·4*	*11·8 ± 1·0*	*57 ± 5*	*5·77*	*71·5 ± 4·4*
NR-A1	60	19	7·2 ± 0·6	14·2 ± 1·0	51 ± 5	5·86	68·1 ± 3·8
NR-2MP	50	11	11·2 ± 0·5	17·6 ± 2·0	64 ± 6	5·81	67·7 ± 3·6
SN-B1	50	16	11·1 ± 0·6	19·5 ± 2·0	61 ± 6	5·64	79·5 ± 4·2
SN-B1B	65	22	6·6 ± 0·6	14·4 ± 1·0	50 ± 5	6·07	80·2 ± 3·6
SN-B3	40	29	12·2 ± 0·9	23·8 ± 2·0	55 ± 5	5·26	74·3 ± 4·0
SN-B4	40	28	8·8 ± 0·0	23·8 ± 2·0	42 ± 4	5·58	75·8 ± 3·9
SN-B5	55	33	8·8 ± 0·7	17·6 ± 1·0	54 ± 4	5·94	83·7 ± 4·4
SN-B6	60	24	11·8 ± 0·3	16·0 ± 1·0	76 ± 3	5·94	71·5 ± 3·3
H2B1	70	26	3·5 ± 0·4	7·2 ± 1·0	53 ± 8	5·43	76·9 ± 3·7
H2B2	60	21	6·5 ± 0·6	16·0 ± 1·0	46 ± 5	4·91	71·6 ± 3·8
Lowland mean	58	19	9·1 ± 0·5	16·6 ± 2·0	57 ± 6	5·59	73·4 ± 3·9

[a] Values in parenthesis represent sampling depth.
[b] SPR values from Heimsath *et al*. (2006).
[c] Not factored into the mean.
Note: Values in italics are samples collected from convergent portions of the landscape.

trace elements likely occurs in both directions across the soil–saprolite boundary: the downward flow of meteoric waters carrying solutes into the saprolite may somewhat balance the upward physical mobilization of saprolite into the soil column by mechanical processes such as tree-throw and burrowing animals and insects. The saprolite mobilized into the soil column experiences further chemical weathering as well as increased physical weathering, thereby delivering solutes via meteoric waters back into the saprolite column.

At the base of the escarpment, our interpretation of soil column thickness versus saprolite CDF agree with those of Green *et al*. (2005). That study, from the same site, determined that chemical weathering accounts for 35% to 55% of total denudation. Similar percentages of total denudation in both the saprolite and the soil suggest that the steady-state assumption used by Heimsath *et al*. (1997) for the general theory of soil production and by Heimsath *et al*. (2000, 2001, 2006) for the fieldsites in south-eastern Australia are further validated.

Samples from divergent regions of the highland site (FH), where slope-dependent transport processes of soil are thought to be dominant over any potential overland flow processes, show an increase in the saprolite chemical weathering rate with increasing slope (Figure 4a). Samples from the lowlands (NR and SN) show a general decline of chemical weathering rates with increasing slope. In the case of the highlands, high chemical weathering rates correspond to steeper slopes where physical weathering processes may dominate and limit soil column thicknesses. A 10° slope may be the critical slope angle above which physical processes dominate the chemical, as suggested by the inflection point revealed when data from all sites are plotted together (Figure 4a).

The abrasion pH plotted against slope angle (Figure 4b) does not show clear trends common to all three sites. Data from individual sites are revealing, however: at the upland site (FH), pH subtly increases from 5 to 6 as the slope angle increases above 10°. This decrease in chemical weathering extent suggests that increasing slope angle above 10° promotes subsurface precipitation runoff and limits groundwater infiltration. Slope angles below 10° show pH values varying from 5·5 to 7·5 with no trend, suggesting the stochastic nature of meteoric water infiltration through the soil and saprolite. An alternate interpretation of upland chemical weathering extent, as measured by abrasion pH, is that the lower chemical weathering intensities (higher pH values) at lower slope

DOI: 10.1002/esp

Table IV. Concentrations of major and trace elements, pH, and CIA at Frog's Hollow

Boring number–depth (cm)	Al_2O_3 (%)	CaO (%)	Fe_2O_3 (%)	K_2O (%)	P_2O_5 (%)	Na_2O (%)	SiO_2 (%)	TiO_2 (%)	LOI (%)	Zr (ppm)	Th (ppm)	Ce (ppm)	pH	CIA
FH-B1-096	14·33	1·56	3·69	3·38	0·06	2·31	70·99	0·38	2·28	117	18	74	6·96	65·60
FH-B1-120	14·48	1·70	3·40	3·31	0·05	2·39	69·42	0·35	2·46	110	17	80	7·27	65·66
FH-B1-180	14·50	1·82	3·80	3·39	0·07	2·52	70·38	0·4	2·02	124	21	85	6·71	64·79
FH-B1-280	13·87	1·91	3·76	3·20	0·09	2·57	71·28	0·41	1·70	120	17	69	6·9	64·12
FH-B1-310	14·15	1·90	3·28	3·10	0·08	2·57	69·88	0·32	2·09	115	17	60	7·15	64·90
FH-B1-340	13·28	1·74	3·11	3·07	0·07	2·41	71·45	0·39	2·29	110	14	50	7·02	64·37
FH-B1-370	13·37	1·68	3·54	3·33	0·09	2·52	72·28	0·39	1·65	123	22	93	7·08	63·12
FH-B1-440	12·96	1·63	2·47	3·06	0·06	2·42	72·97	0·22	1·80	112	22	70	7·38	63·81
FH-B1-500	13·66	1·87	3·39	3·20	0·08	2·68	72·12	0·36	1·60	119	21	78	6·89	63·24
FH-B1-701	14·11	1·44	3·98	3·50	0·10	2·92	70·36	0·42	1·93	136	31	161	7·04	62·00
FH-B1-870	14·17	1·92	4·05	3·27	0·10	2·98	70·10	0·43	1·78	141	26	105	6·91	62·47
FH-B1-1050	14·03	1·84	4·08	3·40	0·09	2·78	70·30	0·44	1·83	147	27	107	7·22	62·77
FH-B1-1175	13·59	1·56	3·71	3·72	0·09	2·59	71·55	0·38	1·66	118	27	147	6·97	61·96
FH-B1-1330	11·22	1·51	2·05	3·11	0·05	2·67	77·88	0·16	0·75	95	12	37	6·96	58·95
FH-B1B-2·4	13·19	2·53	3·22	3·04	0·07	2·63	71·17	0·31	0·79	134	22	70	—	63·13
FH-B1B-23·3	13·8	0·55	0·59	3·85	0·02	4·51	74·50	0·01	0·39	86	55	30	—	54·31
FH-B2-100	13·94	2·08	4·06	3·24	0·07	2·39	70·70	0·43	1·77	140	23	107	7·3	64·98
FH-B2-270	15·03	2·11	3·77	2·95	0·04	2·63	69·92	0·39	2·17	124	18	91	6·91	66·44
FH-B2-430	13·76	2·11	3·90	3·14	0·07	2·55	71·24	0·42	1·59	126	18	86	7·56	64·22
FH-B2-570	13·56	2·29	4·31	3·12	0·07	2·85	71·01	0·36	1·27	137	21	82	7·48	62·47
FH-B2-720	13·31	2·28	4·14	3·24	0·07	2·71	71·75	0·33	1·07	137	15	65	7·59	62·33
FH-B2-870	14·16	2·51	3·28	3·05	0·11	3·14	71·21	0·33	0·97	119	17	73	7·67	62·33
FH-B2-1020	13·62	2·53	3·45	3·07	0·07	2·90	71·91	0·37	0·92	113	17	86	7·58	62·47
FH-B2-1170	13·39	2·33	3·29	3·16	0·07	2·84	72·60	0·32	0·96	115	20	71	7·67	62·09
FH-B2-1405	13·87	2·63	4·00	3·30	0·09	2·91	70·36	0·44	1·01	129	27	104	8·12	62·14
FH-B3-120	13·36	1·48	3·62	3·48	0·04	2·01	72·61	0·39	2·08	150	18	65	7·62	65·22
FH-B3-260	13·82	1·71	3·61	3·09	0·07	2·74	71·90	0·37	1·64	119	21	89	7·36	63·59
FH-B3-420	14·07	1·58	3·90	3·54	0·08	2·66	70·89	0·40	1·74	141	23	94	7·33	62·99
FH-B3-570	13·55	1·06	3·57	3·79	0·06	3·03	71·94	0·36	1·55	128	20	71	7·35	59·75
FH-B3-650	13·35	0·95	3·37	3·62	0·07	3·60	72·36	0·37	1·33	120	20	89	7·64	57·47
FH-B4-120	13·56	1·63	3·88	3·27	0·03	2·07	72·06	0·42	2·14	218	21	65	7·27	65·95
FH-B4-270	14·92	1·38	4·12	3·55	0·08	2·94	69·24	0·44	2·06	141	24	89	7·71	63·08
FH-B4-420	14·35	1·59	3·60	3·31	0·07	2·81	70·97	0·40	1·85	120	24	84	7·62	63·46
FH-B4-505	13·86	2·06	3·64	3·05	0·08	2·67	71·48	0·39	1·67	126	22	91	7·31	64·09
FH-B4-570	13·59	1·73	3·50	3·18	0·07	2·70	72·30	0·36	1·54	130	19	88	7·12	63·10
FH-B5-060	16·71	1·32	4·45	3·60	0·02	1·79	66·83	0·48	3·76	131	24	73	7·45	70·81
FH-B5-120	14·96	1·55	4·34	3·36	0·07	2·34	66·63	0·46	3·77	130	18	90	7·32	66·48
FH-B5-160	14·15	1·88	3·68	3·08	0·07	2·36	71·32	0·39	2·06	111	17	76	7·47	66·02
FH-B5-220	14·04	1·26	3·59	2·87	0·08	2·89	69·88	0·39	2·98	125	20	80	7·57	63·97
FH-B5-250	14·22	1·51	3·91	2·92	0·08	3·08	70·76	0·43	2·00	134	21	89	6·51	63·19
FH-B5-350	13·88	1·11	6·05	3·40	0·07	2·72	69·00	0·41	2·32	127	21	80	5·08	62·87
FH-B5-465	14·44	1·33	4·03	3·68	0·07	2·85	70·13	0·41	1·99	133	20	90	6·98	62·35
FH-B5-410	13·86	1·04	3·46	3·10	0·08	3·12	70·02	0·37	2·58	130	20	70	6·95	61·91
FH-B5-440	14·04	1·05	3·57	3·14	0·08	3·09	69·72	0·45	2·77	121	20	80	7·08	62·23
FH-B5-490	14·38	1·21	3·62	3·36	0·08	2·62	68·95	0·37	2·93	119	20	80	7·50	64·27
FH-B5-575	13·62	0·97	2·27	4·01	0·05	2·91	74·01	0·19	1·29	84	20	77	7·31	59·78
FH-B5-605	13·63	0·99	2·23	3·91	0·04	2·96	74·07	0·20	1·31	94	19	76	7·54	59·87

angles (<10°) are the result of decreasing soil column thicknesses as slope angle increases. This alternate interpretation is consistent with the interpretation of saprolite CDF data. The data from beneath the escarpment are consistent with the upland site in that all sites show that chemical weathering extent is consistently greater at slope angles >10°.

The saprolite CDF plotted against slope angle (Figure 4c) shows no common trends across the three sites but is instructive of processes at individual locations along the escarpment. At the upland site, CDF increases steeply between 0° and approximately 15° combined with the slightly decreased chemical weathering extent suggested by Figure 4(b) further suggest the primacy of physical weathering processes (in this case, biomechanical disturbance and overland flow) on increasing slope angle across the escarpment.

In the discussions of Figures 3 and 4, we have suggested that increased slope angle increases physical processes and limits soil column thickness development. Figure 5 shows slope plotted against soil column thickness for the pit samples shown in Table II. The data distribution in Figure 5 is important to discuss. We sampled three individual hillslopes with similar morphology, and our sampling strategy inherently minimized potential variation in hillslope angles. Median slope angles at all sites are between 10° and 20° and few sample locations have gently sloped to flat locations (<5°) or steep (greater than 25°) slope angles. In general, soil thicknesses appear to average 50 cm. Movement of soil from the hillcrest downslope towards steeper regions could result in higher soil column thicknesses downslope, but we do not observe this at our sites. Instead, steeper slopes may promote further downslope transport of soil and organic material to the convergent and unchanneled swales where the material is periodically evacuated, potentially by extreme events that we have not observed. If this is the case and there is indeed a convergence of soil thicknesses

DOI: 10.1002/esp

Table V. Concentrations of major and trace elements, pH, and CIA at Nunnock River

Depth (m)	Al_2O_3 (%)	CaO (%)	Fe_2O_3 (%)	K_2O (%)	P_2O_5 (%)	Na_2O (%)	SiO_2 (%)	TiO_2 (%)	Zr (ppm)	Th (ppm)	Ce (ppm)	pH	CIA
0·05	13·90	0·74	3·16	3·66	0·03	1·50	78·70	0·51	335	5	16	5·86	67·00
0·25	12·94	0·76	3·87	2·98	0·02	1·20	71·47	0·50	226	NA	NA	6·02	69·24
0·45	15·16	0·72	4·53	3·15	0·02	2·00	66·40	0·53	180	NA	NA	6·94	71·70
0·95	15·60	0·72	5·42	2·39	0·03	2·20	73·10	0·63	176	9	51	6·75	76·72
1·15	14·70	1·21	4·74	2·55	0·02	1·90	66·54	0·69	178	NA	NA	6·97	72·61
1·35	15·08	1·44	4·56	2·91	0·02	2·06	66·71	0·65	167	NA	NA	6·99	70·23
1·65	13·62	1·38	4·60	2·46	0·02	1·80	69·04	0·59	147	NA	NA	6·11	70·92
2·25	15·80	1·69	5·25	3·15	0·03	2·30	72·70	0·67	246	16	66	6·49	69·10
2·55	12·61	1·72	2·62	1·95	0·05	1·99	73·10	0·35	102	NA	NA	6·19	71·11
2·85	13·68	0·83	3·83	2·58	0·04	1·94	68·06	0·43	125	NA	NA	6·19	72·58
3·05	15·50	1·06	4·28	2·78	0·06	2·40	72·80	0·53	159	13	68	6·43	72·93
3·75	13·76	1·50	2·70	2·47	0·05	2·55	71·81	0·33	112	NA	NA	6·76	70·58
4·05	14·90	1·56	4·01	2·61	0·07	2·70	75·00	0·55	189	12	46	6·58	71·19
4·25	13·09	0·68	4·82	2·63	0·04	1·86	67·04	0·45	147	NA	NA	6·70	72·03
4·45	14·10	0·37	5·29	3·49	0·03	1·19	63·64	0·53	172	NA	NA	6·31	69·62
4·65	15·60	0·75	5·05	4·00	0·09	2·20	71·70	0·57	206	15	73	5·90	67·79
6·10	15·60	2·42	4·06	2·74	0·13	2·80	72·70	0·51	147	14	82	6·23	68·42
7·35	14·50	2·34	3·34	2·95	0·10	2·80	75·90	0·41	160	9	50	7·05	66·03
7·65	14·26	2·27	4·87	2·70	0·11	2·38	67·77	0·59	200	NA	NA	7·26	67·17
8·05	13·25	1·88	1·53	2·25	0·05	2·44	74·52	0·16	74	NA	NA	6·70	69·57
8·35	14·70	2·11	3·90	2·88	0·11	3·00	74·40	0·48	164	9	57	6·85	67·47
8·65	15·19	1·76	4·07	3·21	0·10	2·67	65·47	0·55	160	NA	NA	7·31	67·72
9·65	13·90	1·83	4·11	2·66	0·14	2·30	74·70	0·58	208	12	68	7·14	68·44
10·45	15·50	1·31	4·52	3·20	0·14	2·30	72·50	0·61	225	15	98	7·34	69·76
10·65	13·55	1·06	4·04	2·93	0·10	2·58	68·77	0·51	164	NA	NA	7·31	69·31
12·00	15·20	1·38	4·51	3·20	0·13	2·50	71·60	0·56	185	17	98	7·40	69·10
12·20	12·53	1·13	2·93	2·56	0·06	2·19	72·45	0·25	106	NA	NA	7·26	69·61
14·25	15·50	0·59	9·21	3·05	0·09	1·10	67·40	0·36	178	12	246	6·95	73·21
14·50	13·73	1·98	4·01	2·84	0·10	2·17	68·75	0·54	174	NA	NA	7·47	66·63
14·80	13·16	1·79	3·44	2·77	0·09	2·02	70·12	0·48	141	NA	NA	7·30	66·77
15·00	14·20	2·08	3·57	2·85	0·11	2·30	74·70	0·46	141	16	70	7·50	66·97
15·20	13·42	2·13	2·96	2·52	0·07	2·19	70·94	0·33	106	NA	NA	7·41	67·31
17·05	15·00	1·96	3·93	3·00	0·11	2·50	72·60	0·49	144	9	40	7·03	67·82
17·30	15·20	1·84	3·71	3·06	0·11	2·50	73·90	0·52	176	11	47	6·65	68·22

around 50 cm, then the potential exists for the landscapes to have uniform soil depths reflecting long-term equilibrium lowering.

We have established the likely dominance of physical weathering processes at the hillslope scale at our sites. At this scale, chemical weathering rate may be regulated by the availability of water. At the regional scale across the escarpment, physical weathering processes are still likely controlling chemical weathering processes. The availability of water is set not only by soil and lithologic conditions in the saprolite, but also by climatic differences across the region. We move our investigation from bulk saprolite weathering to variations through the entire saprolite profile.

Saprolite columns across the escarpment

We drilled a total of eight borings across the escarpment with a truck-mounted drill rig: five at Frog's Hollow in the highlands (Table IV) and three in the lowlands with one at Nunnock River (Table V) and two at Snug (Table VI). We calculated chemical weathering intensities from major and trace elemental data collected from the borings across the escarpment.

The CIA values plotted against depth (Figure 6) from each of the three sites capture the differences between the sites, yet hint at the complexity of the chemical weathering story across the escarpment. At the highlands site, CIA values are consistent but highly variable in the low sixtires between the surface and water table at 8 m. In the borings that penetrate below 8 m, CIA values are consistent except within 2 to 3 m of the borehole bottom. At the escarpment base, CIA values decrease from the low seventies to the mid-sixties from the surface to approximately 9 m below ground surface. From 9 m to the bottom of the core, CIA values are roughly constant in the mid-sixties. At the lowlands site towards the coast, we find that CIA values decrease from the low seventies to the low sixties down the borehole from the surface to approximately 6 m. Below 6 m depth, CIA values are consistent in the mid-sixties. The CIA results across the escarpment were surprising: the chemical weathering extent at the base of the escarpment, supposedly the least tectonically mature landscape of the three sites, is higher than that from the highlands site. The most likely interpretation of this data rests in the disparity between what the CIA measures and the relationships that exist between primary and secondary minerals in the saprolite columns. Water availability and chemical weathering driven by the present climatic regime have overprinted any signature commensurate with landscape maturity related to the evolution of the escarpment.

Abrasion pH data plotted against depth (Figure 7) from the three sites show decreasing weathering extent with increasing depth. At the highlands site, pH values around 7 are roughly consistent with depth until a slight tail towards higher pH at the bottom of boring B2. At the base of the escarpment in the lowlands, the pH data show an increase from 6 to 7·5 down-profile. The mean trend of pH values also suggests a higher

DOI: 10.1002/esp

Table VI. Concentrations of major and trace elements, pH, and CIA at Snug

Boring number–depth (cm)	Al_2O_3 (%)	CaO (%)	Fe_2O_3 (%)	K_2O (%)	P_2O_5 (%)	Na_2O (%)	SiO_2 (%)	TiO_2 (%)	Ce (ppm)	Th (ppm)	Zr (ppm)	pH	CIA
SN-H2B1-0·4	15·11	0·71	5·27	2·16	0·03	1·25	65·63	0·64	NA	NA	155	5·43	75·40
SN-H2B1-1·0	14·75	0·85	4·62	2·32	0·02	1·96	67·28	0·56	131	11	169	5·96	71·20
SN-H2B1-2·0	15·78	1·31	4·85	2·71	0·04	1·97	65·22	0·55	NA	NA	169	6·38	70·41
SN-H2B1-2·1	14·70	0·98	4·59	2·70	0·06	2·13	67·49	0·54	NA	NA	181	6·27	68·44
SN-H2B1-3·2	15·08	1·90	4·55	2·49	0·06	2·14	67·35	0·51	199	16	148	6·47	69·97
SN-H2B1-3·3	15·79	2·87	8·28	1·74	0·11	1·91	59·65	1·03	126	9	113	6·50	75·88
SN-H2B1-4·0	14·95	1·66	4·81	2·83	0·08	2·10	66·64	0·53	NA	NA	147	6·91	68·17
SN-H2B1-4·2	NA	NA	NA	NA	NA	NA	NA	NA	189	16	176	6·62	NA
SN-H2B1-4·9	13·92	1·60	4·23	2·68	0·08	2·26	68·74	0·49	105	15	151	6·80	66·84
SN-H2B1-5·5	14·32	2·74	5·22	2·72	0·36	2·27	65·41	0·64	133	13	150	6·89	67·15
SN-H2B1-5·6	14·08	2·37	4·22	2·59	0·1	2·37	68·54	0·48	133	14	165	7·02	67·11
SN-H2B1-7·0	NA	NA	NA	NA	NA	NA	NA	NA	68	9	134	7·31	NA
SN-H2B1-8·6	NA	NA	NA	NA	NA	NA	NA	NA	81	14	161	7·05	NA
SN-H2B1-9·3	NA	NA	NA	NA	NA	NA	NA	NA	83	11	157	7·30	NA
SN-H2B2-0·5	16·39	0·45	5·43	3·13	0·04	1·92	62·49	0·69	NA	NA	224	4·91	69·36
SN-H2B2-1·1	14·50	0·68	4·61	2·68	0·04	2·13	67·06	0·57	NA	NA	164	5·42	68·28
SN-H2B2-1·2	14·89	0·77	4·79	2·69	0·05	2·12	66·10	0·59	NA	NA	181	5·59	68·83
SN-H2B2-2·4	14·36	1·59	5·08	2·73	0·11	2·09	66·64	0·58	NA	NA	169	5·90	67·86
SN-H2B2-2·9	13·77	1·70	3·47	2·96	0·08	2·23	69·67	0·42	NA	NA	116	6·29	65·24
SN-H2B2-3·5	14·72	2·38	5·47	2·82	0·12	2·15	64·65	0·69	NA	NA	200	6·32	67·65
SN-H2B2--3·7	13·39	1·44	2·67	4·22	0·07	2·05	71·21	0·33	NA	NA	96	6·69	59·26
SN-H2B2-4·2	13·94	1·97	4·43	2·84	0·1	2·30	67·78	0·55	NA	NA	170	5·84	65·87
SN-H2B2-4·3	NA	NA	NA	NA	NA	NA	NA	NA	101	11	148	6·34	NA
SN-H2B2-5·1	14·04	1·59	5·09	2·83	0·12	2·77	66·91	0·61	NA	NA	180	6·50	64·58
SN-H2B2-5·2	NA	NA	NA	NA	NA	NA	NA	NA	166	17	166	6·90	NA
SN-H2B2-5·3	14·39	1·27	4·41	2·30	0·1	4·31	67·01	0·50	142	14	140	7·12	62·90
SN-H2B2-5·8	14·34	1·58	4·73	2·50	0·11	2·77	67·56	0·54	157	17	184	7·01	66·70
SN-H2B2--6·0	14·18	1·35	5·62	1·60	0·13	4·01	65·39	0·69	110	19	187	6·93	66·91
SN-H2B2-6·6	NA	NA	NA	NA	NA	NA	NA	NA	131	17	170	7·37	NA
SN-H2B2-7·3	14·61	1·56	5·06	1·85	0·1	3·65	65·73	0·60	97	15	139	6·59	67·48
SN-H2B2--7·5	14·62	1·40	4·32	2·04	0·1	3·80	67·69	0·54	NA	NA	173	6·97	66·06
SN-H2B2-12·8	NA	NA	NA	NA	NA	NA	NA	NA	121	14	149	6·75	NA
SN-H2B2-16·4	18·55	1·08	6·72	0·25	0·13	7·30	57·66	0·65	44	7	136	7·89	68·97
SN-H2B2-17·5	NA	NA	NA	NA	NA	NA	NA	NA	161	19	207	7·73	NA
SN-H2B2-17·8	19·07	0·90	5·66	0·25	0·13	8·09	58·91	0·51	NA	NA	162	7·94	67·47
SN-H2B2-18·2	18·72	1·49	5·86	0·08	0·15	8·20	57·90	0·75	NA	NA	214	8·21	67·41
SN-H2B2-18·45	18·81	1·37	6·08	0·10	0·14	8·04	58·51	0·66	NA	NA	191	7·99	67·86
SN-H2B2-19·3	19·00	1·04	5·54	0·04	0·16	8·38	58·65	0·81	NA	NA	238	7·41	67·46
SN-H2B2-20·8	18·66	0·62	5·46	0·11	0·12	8·00	59·14	0·60	NA	NA	208	7·26	67·81
SN-H2B2-22·2	19·32	0·63	7·03	0·22	0·14	7·46	56·07	0·78	NA	NA	210	7·54	69·56

Table VII. Cation concentrations at FH and NR·(all concentrations in μg l^{-1})

Sample	Na	Mg	Al	Si	K	Ca	Mn	Fe	Rb	Sr	Total
FH	9035	2640	72	9575	494	5697	0·89	158	0·53	29·8	27702
NR	9397	2003	1·5	12890	904	4041	<0·2	<9	0·91	34·0	29272

extent of weathering than at the highland site above the escarpment. The data from the lowlands sites near the coast indicate intense weathering near the surface of the saprolite, but pH values at depth are higher, in agreement with those collected in the highlands and at the escarpment base. As with our interpretation of the higher CIA values at the base of the escarpment, we suggest that abrasion pH values reflecting recent climate and chemical weathering have overprinted longer term weathering effects of escarpment propagation. The more intense weathering shown in upper portions of the cores beneath the escarpment may represent an additional weathering front overprinting an older climate signal as it propagates down through the saprolite profile. The timescale at which recent chemical weathering signatures become dominant over older ones is equivalent to the weathering front propagation rate – both are dependent on the rates at which secondary and, to a lesser extent, primary weathering products dissolve and precipitate.

Because our interpretation of the abrasion pH data plotted against depth from the three sites agrees with that of the CIA data, we compare the abrasion pH measure of chemical weathering extent with that of the CIA (Figure 8). Both a linear function and a second-order polynomial fit to the data indicate rough agreement between the two metrics ($r^2 = 0{\cdot}31$), suggesting both the CIA and abrasion pH methods respond to changes in chemical weathering extent in similar ways and neither method alters its response across the spectrum of chemical weathering intensities.

Concentrations of Zr across the three sites plotted against depth (Figure 9) provide a baseline for interpreting chemical

DOI: 10.1002/esp

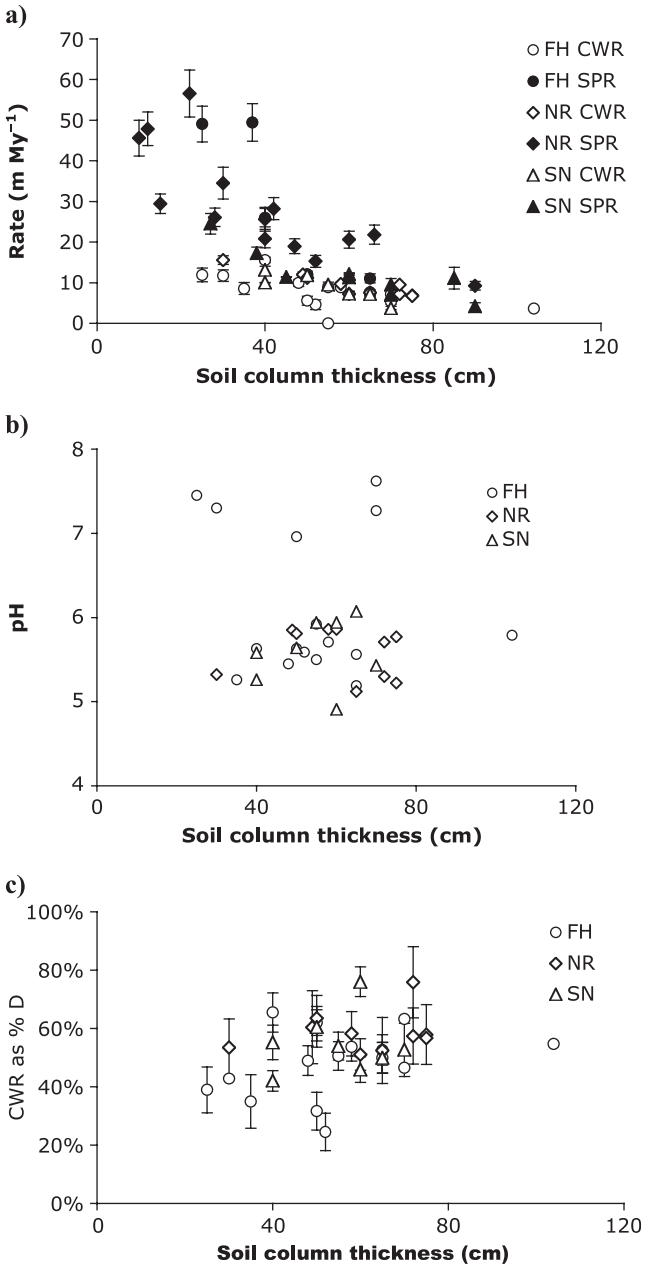

Figure 3. Chemical weathering rate and the soil production rates (a), pH (b), and the CDF (c) are plotted against soil column thickness for samples from convergent and divergent sections of the hillslope. Hollow circles denote FH samples (upland site), hollow diamonds, NR (base of escarpment), and hollow triangles, SN (lowland).

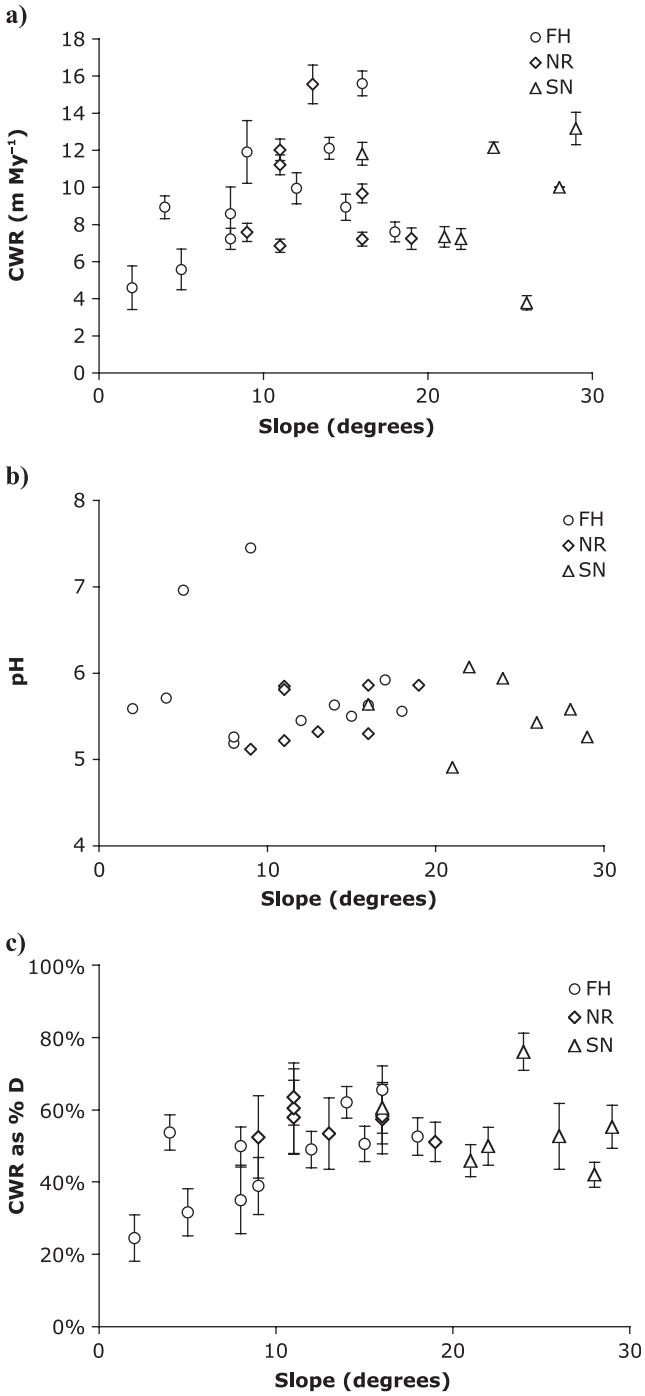

Figure 4. Chemical weathering rates (a), pH (b), and the CDF (c) are plotted against slope for all soil pit samples. Hollow circles denote FH samples (upland site), hollow diamonds, NR (base of escarpment), and hollow triangles, SN (lowland).

weathering rates calculated from the samples as well as a measure of the chemical weathering depletion fractions (Riebe *et al.*, 2001, 2003a). All five borings at the highlands site show uniform Zr values. In the lowlands, at the escarpment base, Zr concentrations show considerable variation. The topmost Zr concentration of 340 mg kg^{-1} reflects conservative enrichment in the soil above the saprolite at the drill site. Towards the coast at the other lowlands site, Zr concentrations subtly trend lower with increasing depth. The Zr concentration at the upland site, versus the higher mean concentrations at the lowland sites, is a result of the differences in mineralogy between the Anembo granodiorite and the Bemboka granodiorites of the lowland sites. It is unlikely that the relative differences are the result of incipient chemical weathering from escarpment propagation.

Measurement of volumetric strain measured relative to Zr, Ce, Th, and Ti within a borehole representative of each site represents the volume change that has occurred within the saprolite (Figure 10). Above the escarpment, volume change above the water table at 4 m depth varies around zero. Below the water table, the data suggests a 50% reduction in volume. This may be the result of compaction and leaching significant enough to inhibit the precipitation of secondary minerals into dissolution cavities. Volume change at the escarpment base also varies around zero except at the surface. We interpret the large variations in strain in the subsurface as the result of fracturing and more intense chemical weathering around those fractures. Large volume changes in surface saprolite at NR may be the result of previous land use disruption, such as a ranch roadcut. At the lowland Snug site, the strain at SN B1

DOI: 10.1002/esp

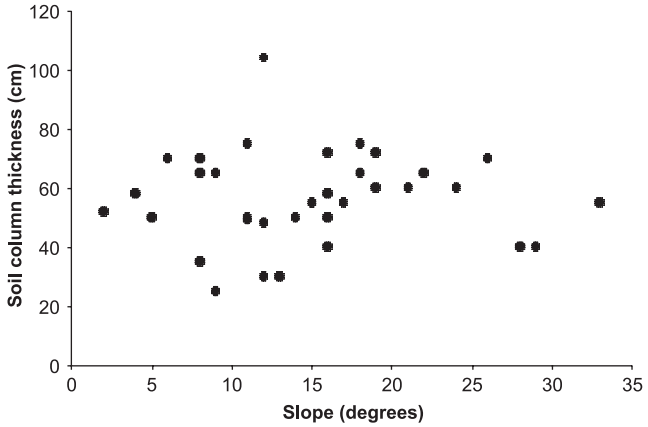

Figure 5. Soil column thickness (in cm) against slope (in degrees) for all pit locations.

with depth shows consistent volume increase in the upper regions of the cores. This result may be the effect of the Zr concentrations in the interfingering granodiorite and adamellite, two parent materials with different weathering characteristics visually observed in the cores.

The figures of major oxide elemental loss with depth (Figure 11) exhibit the values we originally hypothesized for chemical weathering across the escarpment. FH, tectonically the most mature landscape, shows considerable elemental loss both above and below the water table. The profiles at the two lowland sites are similar, with some large gains we again interpret to be the result of significant fractures. At the coastal lowland site, Snug, the difference in apparent elemental gain in the upper and the lower areas is likely the result of lithologic change across the profile.

Saprolite weathering front propagation

Solute chemistries for samples collected above and at the base of the escarpment are presented in Table VII. The samples of riverwater presented in Table VII were taken contemporaneously with the drilling operations. A sample of rainwater was also collected for baseline analysis. Using Equation 9, we determined an approximate catchment-averaged downward propagation rate for the saprolite weathering front into the bedrock at Frog's Hollow above the escarpment of 17 ± 1 m Ma^{-1} and 26 ± 2 m Ma^{-1} at the escarpment base. Although these values are first-order estimates, these saprolite propagation rates are similar to the range of rates reported by Heimsath *et al*. (2000, 2001, 2006) above the escarpment (about 10 to 50 m Ma^{-1}) and across the escarpment face (roughly 4 to 40 m Ma^{-1}).

The conceptual model of chemical weathering in the saprolite and soil (Figure 1) suggests that the production of saprolite is likely to be proportional to the production of soil. Specifically, the presence of a finite saprolite layer (i.e. it is not unweathered bedrock beneath soil, or hundreds of meters of deeply weathered saprolite) hints at a negative feedback between the saprolite propagation and the thickness of the saprolite. Whether this propagation rate is indeed similar to or proportional to the soil production rate is a question that is at the heart of connecting surface weathering processes with longer time scales of landscape evolution. With the limited data that enable an inference of the saprolite propagation rate we cannot currently make this comparison, but we suggest some support for the rates being similar. Namely that the weathering front propagation rate and the associated mass loss from the bedrock as it chemically weathers to saprolite may be similar to the soil production rate.

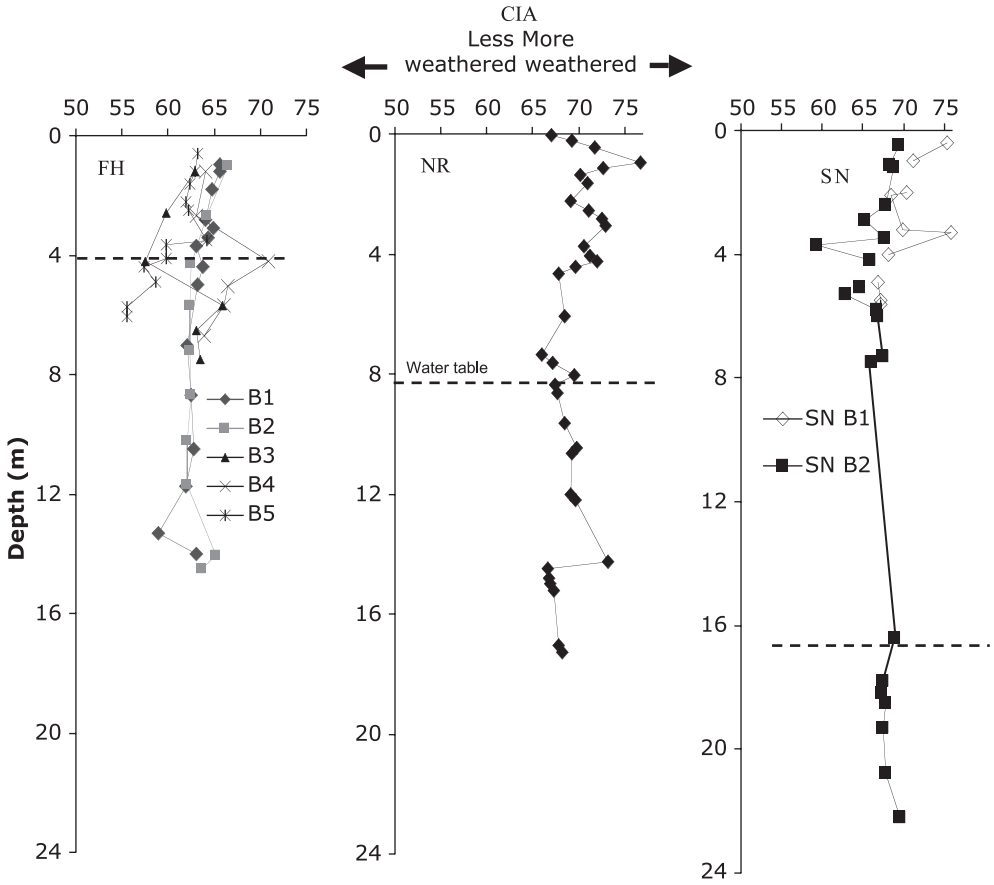

Figure 6. CIA values plotted against depth (in m) for all borings. A CIA value of 60 denotes no weathering; a value near 90 indicates nearly complete chemical weathering of primary minerals.

DOI: 10.1002/esp

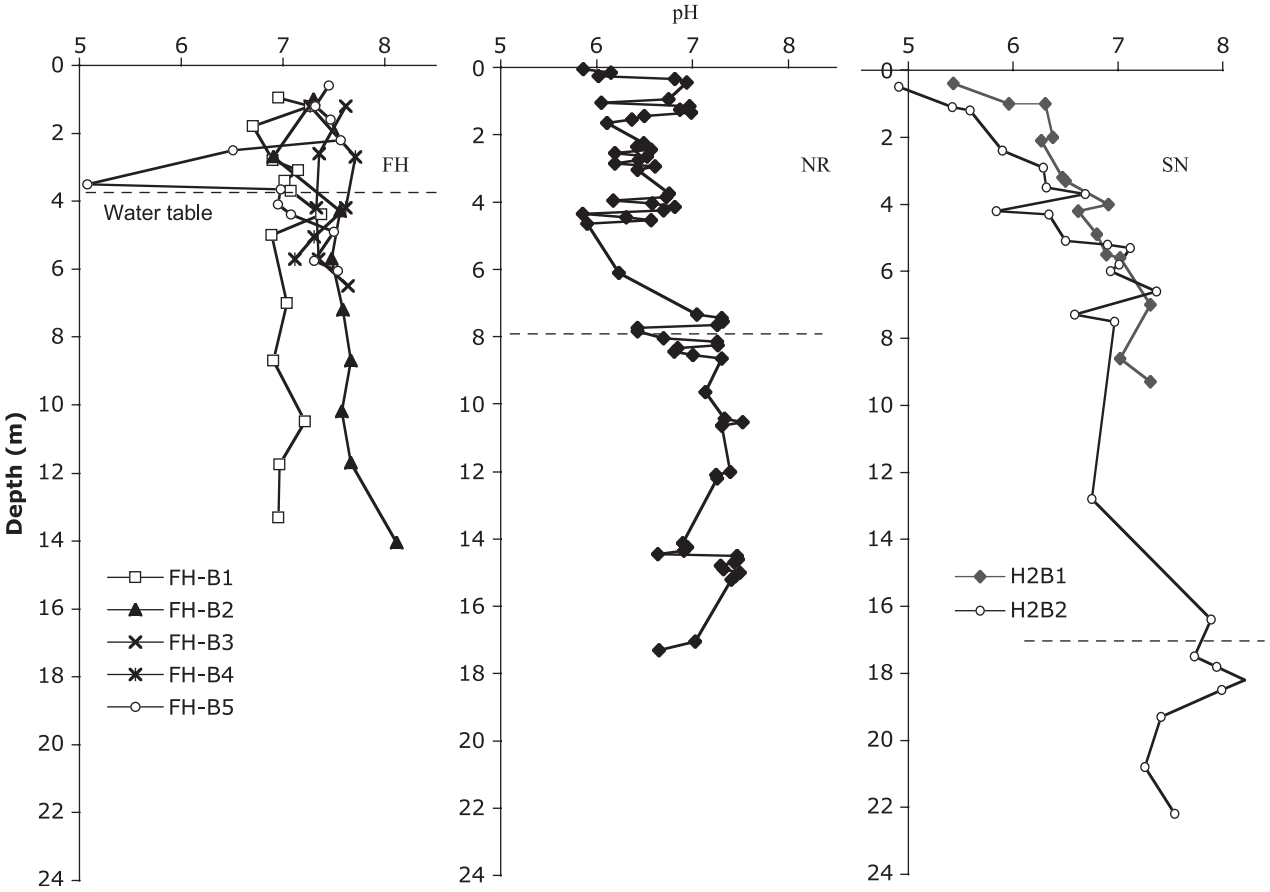

Figure 7. pH, a measure of chemical weathering intensity, plotted against depth (in m).

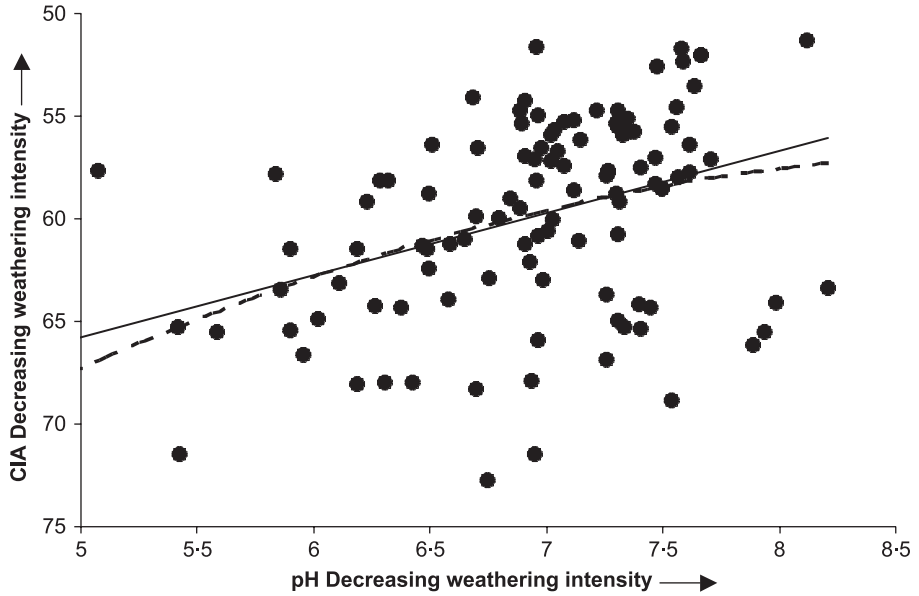

Figure 8. A crossplot of pH and CIA values from core samples at all field locations. Both linear (solid line) and second-order polynomial (dashed line) trendlines shown have $r^2 = 0{\cdot}31$.

Saprolitization, escarpment location, and propagation

The support we find for the steady-state assumption in the theory of soil production is not inconsistent with the likely model of escarpment propagation supported by Persano *et al.* (2002). As long as the relative climatic differences we observe in rainfall and precipitation data have existed through time, the relative differences we find in weathering rates and extents will continue to be present across the escarpment. A careful isotopic study of the saprolite profiles across the escarpment for signatures of past climates and past weathering regimes would, therefore, find similar relative differences in climate and weathering rates.

It is intriguing to find that mean weathering extents in the lowlands ($73{\cdot}7 \pm 3{\cdot}9$) as measured by the CIA are higher than those at the highland site ($65{\cdot}5 \pm 3{\cdot}4$). We expected to find the opposite to be true, given that the highland site is argued

DOI: 10.1002/esp

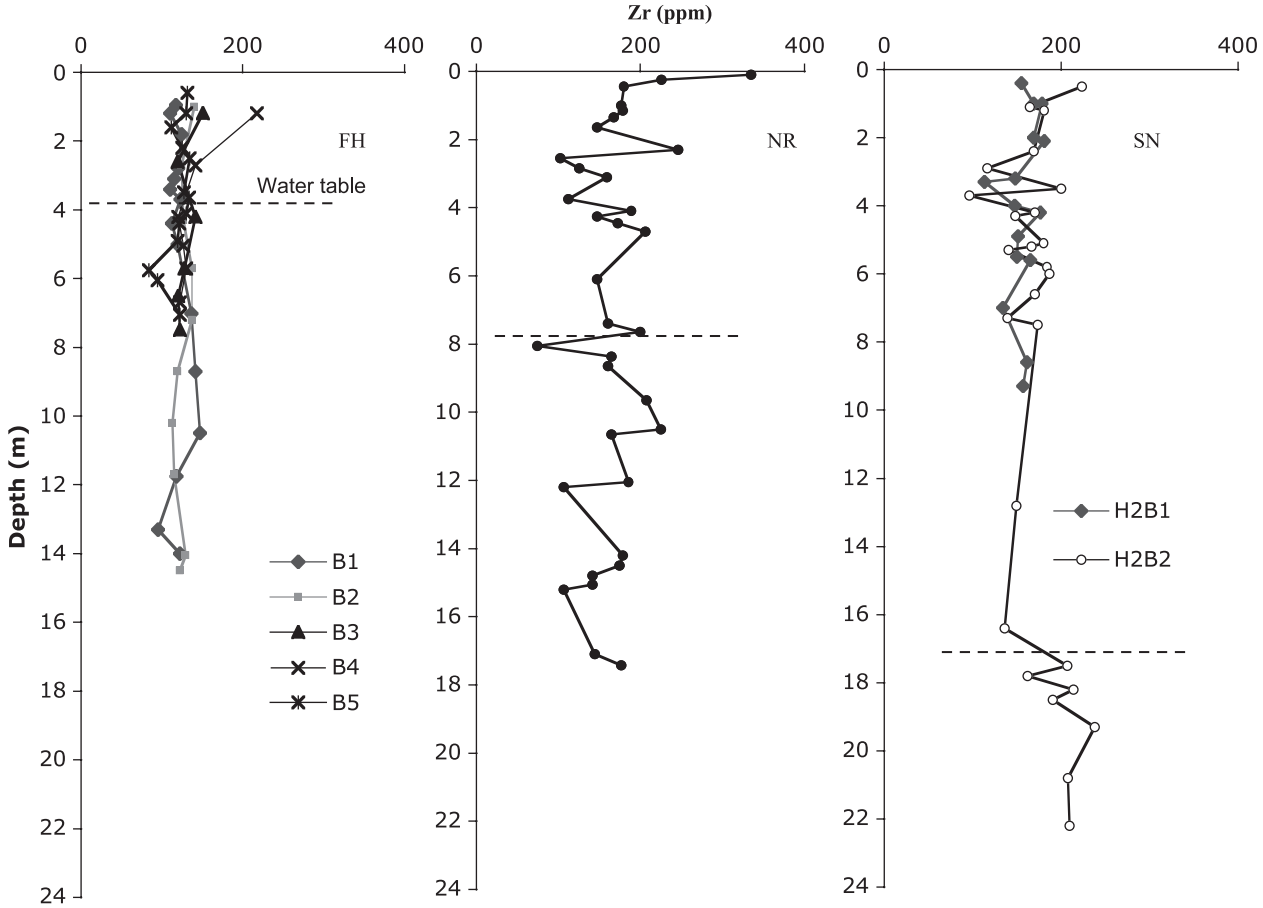

Figure 9. Zr concentrations (in ppm) plotted against depth at all three sites.

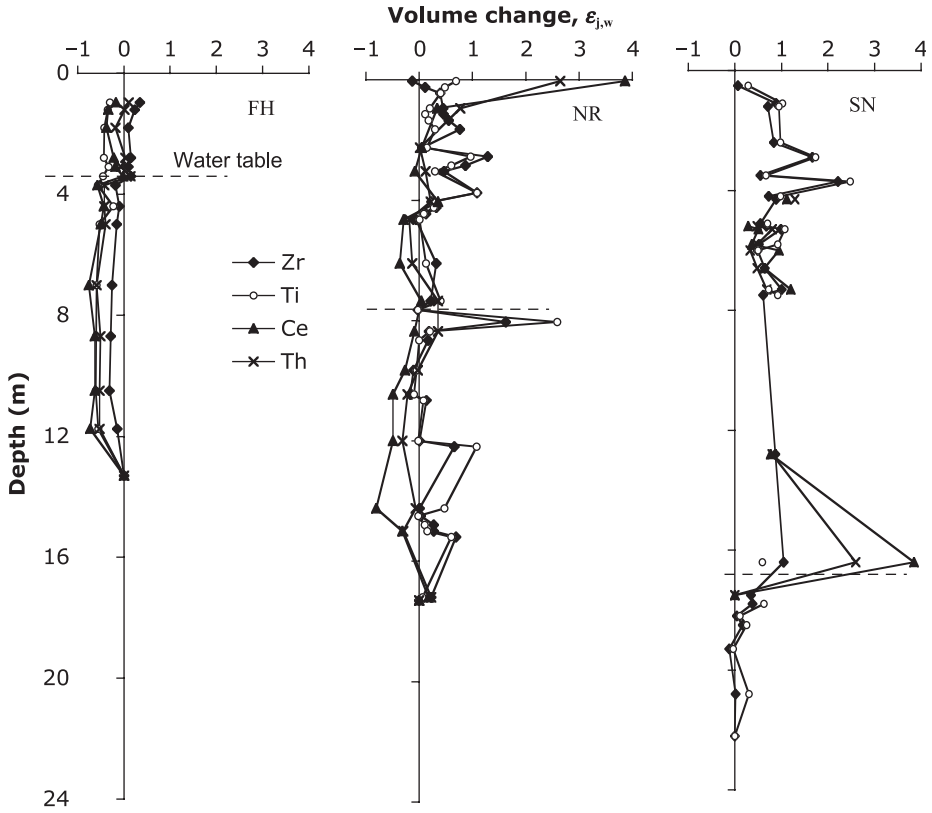

Figure 10. Volume changes (strain) plotted against depth. Compaction and dilation are denoted by values of $\varepsilon_{j,w} < 0$ and $\varepsilon_{j,w} > 0$, respectively. A value of $\varepsilon_{j,w} = 0$ indicates isovolumetric weathering.

DOI: 10.1002/esp

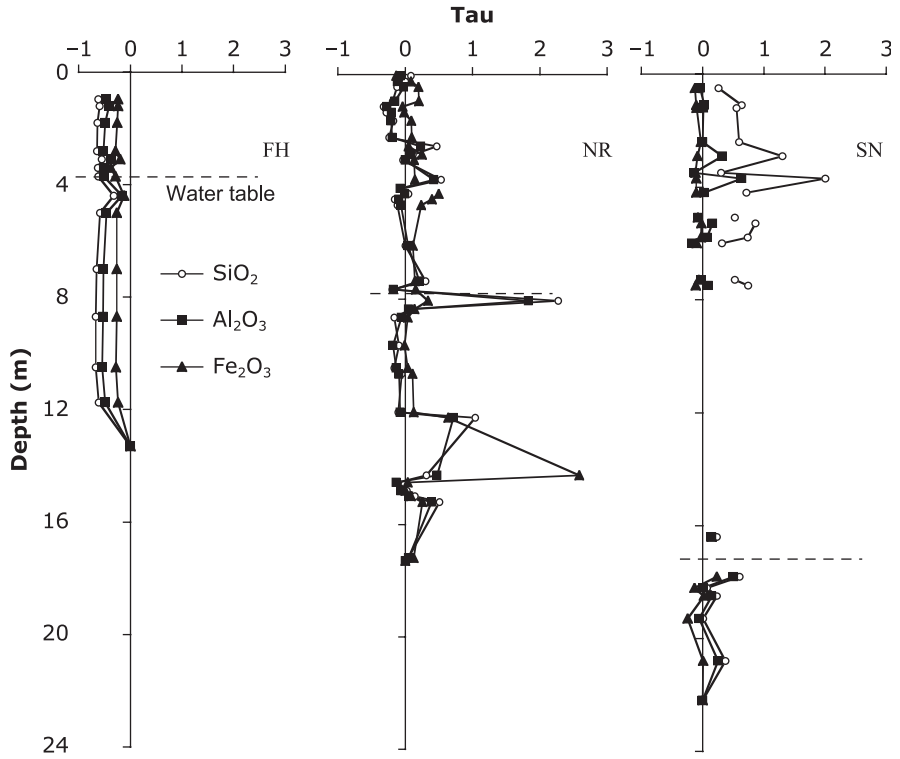

Figure 11. Elemental depletion plotted against depth for SiO_2, Al_2O_3, and Fe_2O_3 at each of the three sites. Values = 0 indicate no elemental loss. Values = –1 indicate complete elemental loss. Values >0 indicate elemental gain.

to be the tectonically older site than either of two lowland sites. We would expect this to be the case even if we accept the Persano *et al*. (2002) model of escarpment propagation that has the escarpment moving quickly after Tasman rifting to its present location. Relatively warmer climate in the lowlands, compared to the highlands, suggests that the effects of present and recent climate regimes have greater influence on saprolite profiles given the denudation rates. This suggestion is similar to the findings of White *et al*. (1996, 1998), Schulz and White (1999), and White (2003), who found that temperature significantly affected weathering.

The difference in chemical weathering extent above and below the escarpment correlates to the precipitation gradient across the escarpment that varies by a factor of two. Furthermore, the thickness of the saprolite column varies as well. While some borings at highland Frog's Hollow met refusal at inferred and confirmed core stones, our deepest boring penetrated two core stones and did not contact bedrock at 38·7 m below ground surface. One boring at the lowland Snug site penetrated 17·4 m before contacting what we believe to be bedrock at a depth also suggested by bedrock outcropping in the adjacent stream channel. In both borings at the lowland site, we found a gradational contact between the bedrock, the deeper boring finding its contact between 19 and 23 m below ground surface. It seems that both precipitation rates and saprolite horizon thickness, then, correlate to chemical weathering extent and as such to the suggested escarpment propagation history.

If saprolite column thickness correlates to escarpment propagation history, chemical weathering extent may be decoupled from the chemical and physical weathering rates, and, furthermore, the proposed steady-state relationship first articulated by Stallard and Edmond (1983) between saprolite formation and physical erosion rates may also be decoupled. The agreement of our measurements of saprolite propagation rates with the observed physical weathering rates from the same fieldsites and areas (Heimsath *et al*., 2000, 2001, 2006) support the coupling of shallow physical and deep weathering processes. White *et al*. (1998) found the saprolite propagation rate at Rio Icacos (58 m Ma^{-1}) was at the upper end of, but in agreement with the long-term denudation rates measured from ^{10}Be accumulations on a nearby ridge (25–50 m Ma^{-1}). Results by Pavich and Obermeier (1989) also agree with the similar rates of surface lowering and deep weathering interface propagation.

Strain and elemental loss rates are affected by the presence of the water table. Stable CIA values below the water table at the highlands site suggest that an equilibrium may exist between groundwater and the surrounding saprolite. Because of the potential kinetic equilibrium between groundwater and saprolite, we conclude that no chemical weathering is occurring beneath the water table. However, gradients in the CIA values with depth at in the lowlands at the base of the escarpment, beneath the water table, and at the lowlands site towards the coast, in the intermittently wet areas, suggest active chemical weathering along zones of preferential flow from fractures. At the escarpment base, there is likely no equilibrium between saprolite and groundwaters, and chemical weathering throughout the saprolite profile remains active.

Conclusions

We used a truck-mounted drill rig to collect samples of saprolite between the soil–saprolite interface and the saprolite–bedrock interface at three fieldsites across the passive margin escarpment of south-eastern Australia. Using major and trace elemental chemistry and pH measurements, we calculated chemical weathering extent using the CIA. We also calculated volumetric strain and elemental change during weathering using mass balance methods. We collected these data to test the hypothesis that the more mature landscape above the escarpment would have more intensely-weathered saprolite and, consequently, the less mature landscape recently exhumed by escarpment propagation would show less intense weathering.

DOI: 10.1002/esp

We found that saprolite horizons below the escarpment show greater chemical weathering intensities and higher chemical weathering rates than does the saprolite horizon in the landscape above it. Although weathering extent correlates with the amount of annual precipitation across the escarpment, the weathering intensities at the base of the escarpment likely reflect a combination of more highly fractured and jointed bedrock and the occurrence of active chemical weathering at these sites. We determined a range of saprolite weathering front propagation rates using watershed solute fluxes and the assumption of isovolumetric weathering in the saprolite and showed that these rates agree closely with the soil production rates calculated previously. The effect of escarpment development and propagation on chemical weathering signatures is likely minimal; it is largely overprinted by the climate gradient across the escarpment. This climate gradient creates distinct chemical weathering signatures in the saprolite column, likely focusing the highest rates and intensities of chemical weathering at the escarpment base.

Acknowledgements—We thank the landowners at the three fieldsites for site access: Rishi Satyadharma at Nunnock River, Les Blake at Frog's Hollow, and Mark Green and his lessees at Snug. Damien Kelleher (ANU) tirelessly operated the truck-mounted drill rig. Tim Allen at Keene State University helped with the XRF analyses. Davidson Vivit at the USGS analyzed the solute chemistry of the water samples. Ron Amundson, Rebecca Fraser, Dylan White, Dave Holliday, Lis Greene, Katya Meyer, Carissa Rodrigue, and Dan Burke provided field assistance. Danielle Moore provided general support. The project was supported by a NSF-EAR-CAREER grant (AMH), a GSA Graduate Fellowship (BCB), and in-kind support from the Research School of Earth Sciences at ANU and the Water Resources Division of the USGS. Burke acknowledges the support of ExxonMobil Development in the publication of the study. We thank Liam Reinhardt and Jason Price for their extensive and helpful reviews.

References

Anderson SPD, William E, Brimhall GH. 2002. Weathering profiles, mass-balance analysis, and rates of solute loss: linkages between weathering and erosion in a small, steep catchment. *Geological Society of America Bulletin* **114**(9): 1143–1158.

Australia B.o.M. 2003. *Climatic Averages for Nimmitabel, NSW, 1894–2003*. http://www.bom.gov.au/climate/averages/tables/cw_070067.shtml [Accessed 21 July 2003, 3 December 2008].

Balan ET, Patrick JJ, Fritsch E, Muller J-P, Calas G. 2001. Surface chemistry of weathered zircons. *Chemical Geology* **181**: 13–22.

Banfield JF, Eggleton RA. 1989. Apatite replacement and rare earth mobilization, fractionation, and fixation during weathering. *Clays and Clay Minerals* **37**(2): 113–127.

Barker WW, Welch SA, Chu S, Banfield JF. 1998. Experimental observations of the effects of bacteria on aluminosilicate weathering. *American Mineralogist* **83**: 1551–1563.

Brimhall GH, Dietrich WE. 1987. Constitutive mass balance relations between chemical composition, volume, density, porosity, and strain in metasomatic hydrochemical systems: results on weathering and pedogenesis. *Geochimica et Cosmochimica Acta* **51**: 567–587.

Brimhall GH, Chadwick OA, Lewis CJ, Compstom W, Williams IS, Danti KJ, Dietrich WE, Power ME, Hendricks D, Bratt J. 1992. Deformational mass transport and invasive processes in soil evolution. *Science* **255**(5045): 695–702.

Brimhall GH, Lewis CJ, Ford C, Bratt J, Taylor G, Warin O. 1991. Quantitative geochemical approach to pedogenesis: importance of parent material reduction, volumetric expansion, and eolian influx in laterization. *Geoderma* **51**: 51–91.

Burke BC, Heimsath AM, White AF. 2007. Coupling chemical weathering with soil production across soil-mantled landscapes. *Earth Surface Processes and Landforms* **32**(6): 853–873.

Carson M, Kirkby MJ. 1972. *Hillslope Form and Process*. Cambridge University Press: New York; 475 pp.

Chadwick OA, Brimhall GH, Hendricks DA. 1990. From black box to grey box: a mass balance interpretation of pedogenesis. *Geomorphology* **3**: 369–390.

Chappell BW, White AJR. 1976. Plutonic rocks of the Lachlan Mobile Zone. *25th International Geological Congress, Sydney, Excursion Guide 13C*, 40 pp.

Cleaves ET. 1974. *Report of Investigations No. 25: Petrologic and Chemical Investigation of Chemical Weathering in Mafic Rocks, Eastern Piedmont of Maryland*. Maryland Geological Survey: Baltimore, MD; 28 pp.

Cleaves ET. 1993. Climatic impact on isovolumetric weathering of a coarse-grained schist in the northern Piedmont Province of the central Atlantic states. *Geomorphology* **8**: 191–198.

Cockburn HAP, Brown RW, Summerfield MA, Seidl MA. 2000. Quantifying passive margin denudation using a combined fission-track thermochronology and cosmogenic isotope analysis approach. *Earth and Planetary Science Letters* **179**: 429–435.

Dietrich WE, Reiss R, Hsu ML, Montgomery DR. 1995. A process-based model for colluvial soil depth and shallow landsliding using digital elevation data. *Hydrological Processes* **9**(3–4): 383–400.

Galloway RW. 1965. Late Quaternary climates in Australia. *Journal of Geology* **73**: 603–618.

Grant WH. 1969. Abrasion pH, an index of chemical weathering. *Clays and Clay Minerals* **17**: 151–155.

Green EG, Dietrich WE, Banfield JK. 2006. Quantification of chemical weathering rates across an actively eroding hillslope. *Earth and Planetary Science Letters* **242**(1–2): 155–169.

Hayes DE, Ringis J. 1973. Seafloor spreading in the Tasman Sea. *Nature (London)* **243**: 454–458.

Heimsath AM, Chappell J, Dietrich WE, Nishiizumi K, Finkel RC. 2000. Soil production on a retreating escarpment in southeastern Australia. *Geology (Boulder)* **28**(9): 787–790.

Heimsath AM, Chappell J, Dietrich WE, Nishiizumi H, Finkel RC. 2001. Late Quaternary erosion in southeastern Australia: a field example using cosmogenic nuclides. *Quaternary International* **83**(5): 169–185.

Heimsath AM, Chappel J, Finkel RC, Fifield K, Alimanovic A. 2006. Escarpment erosion and landscape evolution in southeastern Australia. In *Tectonics, Climate, and Landscape Evolution*, Willet SD, Hovius N, Brandon MT, Fisher DM (eds), Geological Society of America Special Paper 398. The Geological Society of America: Boulder, CO; 173–190.

Heimsath AM, Chappell J, Spooner NA, Questiaux DG. 2002. Creeping soil. *Geology* **30**(2): 111–114.

Heimsath AM, Dietrich WE, Nishiizumi K, Finkel RC. 1997. The soil production function and landscape equilibrium. *Nature (London)* **388**(6640): 358–361.

Heimsath AM, Dietrich WE, Nishiizumi K, Finkel RC. 1999. Cosmogenic nuclides, topography, and the spatial variation of soil depth. *Geomorphology* **27**(1–2): 151–172.

Heimsath AM, Furbish DJ, Dietrich WE. 2005. The illusion of diffusion: field evidence for depth-dependent sediment transport. *Geology* **33**(12): 949–952.

Hoch AR, Reddy MM, Drever JI. 1996. The effect of iron content and dissolved O (sub 2) on dissolution rates of clinopyroxene at pH 5·8 and 25 degrees C; preliminary results. *Chemical Geology* **132**(1–4): 151–156.

Joplin GA. 1963. Chemical analyses of Australian rocks. Pt I: Igneous and metamorphic rocks. Bulletin 65. Bureau of Mineral Resources: Australia; 1–446.

Kim S, Park HD. 2003. The relationship between physical and chemical weathering indices of granites around Seoul, South Korea. *Bulletin of Engineering Geology & Environment* **62**: 207–212.

Kirkwood DE, Nesbitt HW. 1991. Formation and evolution of soils from an acidified watershed: Plastic Lake, Ontario, Canada. *Geochimica et Cosmochimica Acta* **55**: 1295–1308.

Lewis PC, Glen RA, Pratt GW, Clarke I. 1994. *Explanatory Notes: Bega-Mallacoota 1:250 000 Geological Sheet*. Geological Survey of New South Wales: Sydney.

Matmon A, Bierman P, Enzel Y. 2002. Pattern and tempo of great escarpment erosion. *Geology (Boulder)* **30**(12): 1135–1138.

DOI: 10.1002/esp

McDowell WH, Asbury CE. 1994. Export of carbon, nitrogen, and major ions from three tropical montane watersheds. *Limnology and Oceanography* **39**(1): 111–125.

Nesbitt HWY. 1982. Early Proterozoic climates and plate motions inferred from major element chemistry or lutites. *Nature (London)* **299**: 715–717.

O'Sullivan PB, Foster DA, Kohn BP, Gleadow AJW. 1996. Multiple postorogenic denudation events – an example from the eastern Lachlan fold belt. *Geology (Boulder)* **24**: 563–566.

Pavich MJ. 1986. Processes and rates of saprolite production and erosion on a foliated granitic rock of the Virginia Piedmont. In *Rates of chemical weathering of rocks and minerals*, Coldman SM, Dethier DP (eds). Academic Press: Orlando; 551–590.

Pavich MJL, Obermeier SF. 1989. *Investigations of the Characteristics, Origin, and Residence Time of the Upland Residual Mantle of the Piedmont of Fairfax County, Virginia*. US Geological Survey Professional Paper No. 1352. US Geological Survey: Reston, VA; 114 pp.

Persano C, Stuart FM, Bishop P, Barfod DN. 2002. Apatite(U-Th)/He age constraints on the development of the Great Escarpment on the southeastern Australian passive margin. *Earth and Planetary Science Letters* **200**: 79–90.

Price JR, Velbel MA. 2003. Chemical weathering indices applied to weathering profiles developed on heterogeneous felsic metamorphic parent rocks. *Chemical Geology* **202**(3–4): 397–416.

Richardson SJ. 1976. *Geology of the Michelago 1:100 000 sheet 8726*. Geological Survey of New South Wales: Sydney.

Riebe CS, Kirchner JW, Finkel RC. 2003a. Long-term rates of chemical weathering and physical erosion from cosmogenic nuclides and geochemical mass balance. *Geochimica et Cosmochimica Acta* **67**(22): 4411–4427.

Riebe CS, Kirchner JW, Finkel RC. 2003b. Sharp decrease in long-term chemical weathering rates along an altitudinal transect. *Earth and Planetary Science Letters* **6936**: 1–14.

Riebe CS, Kirchner JW, Granger DE, Finkel RC. 2001. Strong tectonic and weak climatic control of long-term chemical weathering rates. *Geology (Boulder)* **29**(6): 511–514.

Schulz MS, White AF. 1999. Chemical weathering in a tropical watershed, Luquillo mountains, Puerto Rico III: Quartz dissolution rates. *Geochimica et Cosmochimica Acta* **63**(3–4): 337–350.

Stallard RF, Edmond JM. 1983. The influence of geology and weathering environment on the dissolved load. *Journal of Geophysical Research* **88**: 9671–9688.

Taunton AE, Welch SA, Banfield JF. 2000a. Geomicrobiological controls on light rare earth element, Y and Ba, distributions during granite weathering and soil formation. *Journal of Alloys and Compounds* (**303–304)**: 30–36.

Taunton AE, Welch SA, Banfield JF. 2000b. Microbial controls on phosphate and lanthanide distributions during granite weathering and soil formation. *Chemical Geology* **169**(3–4): 371–382.

Turner BF, Stallard RF, Brantley SL. 2003. Investigation of in-situ weathering of quartz diorite bedrock in the Rio Icacos basin, Luquillo Experimental Forest, Puerto Rico. *Chemical Geology* **202**(3–4): 313–341.

van der Beek PA, Braun J, Lambeck K. 1999. Post-Palaeozoic uplift history of southeastern Australia revisited; results from a process-based model of landscape evolution. *Australian Journal of Earth Sciences* **46**(2): 157–172.

Weissel JK, Hayes DE. 1977. Evolution of the Tasman Sea reappraised. *Earth and Planetary Science Letters* **36**(1): 77–84.

Welch SA, Banfield JF. 2002. Modification of olivine surface morphology and reactivity by microbial activity during chemical weathering. *Geochimica et Cosmochimica Acta* **66**(2): 213–221.

Welch SA, Banfield JF. 2002. Effect of microorganisms and microbial metabolites on apatite dissolution. *Geomicrobiology Journal* **19**: 343–367.

Welch SA, Barker WW, Banfield JF. 1999. Microbial extracellular polysaccharides and plagioclaise dissolution. *Geochimica et Cosmochimica Acta* **63**(9): 1405–1419.

White AF. 2002. Determining mineral weathering rates based on solid and solute weathering gradients and velocities: application to biotite weathering in saprolites. *Chemical Geology* **190**: 69–89.

White AF. 2003. Weathering and the biosphere. *Geochimica et Cosmochimica Acta* **67**(18): A350.

White AF, Blum AE, Bullen TD, Harden JW, Peterson ML. 1996. Chemical weathering rates of a soil chronosequence on granitic alluvium; I. Quantification of mineralogical and surface area changes and calculation of primary silicate reaction rates. *Geochimica et Cosmochimica Acta* **60**(14): 2533–2550.

White AF, Blum AE, Bullen TD, Vivit DV, Schulz MS, Fitzpatrick J. 1999. The effect of temperature on experimental and natural chemical weathering rates of granitoid rocks. *Geochimica et Cosmochimica Acta* **63**(19–20): 3277–3291.

White AF, Blum AE, Schulz MS, Vivit DV, Stonestrom DA, Larson M, Murphy SF, Eberl D. 1998. Chemical weathering in a tropical watershed, Luquillo Mountains, Puerto Rico; I. Long-term versus short-term weathering fluxes. *Geochimica et Cosmochimica Acta* **62**(2): 209–226.

White AF, Brantley SL. 2003. The effect of time on the weathering of silicate minerals: why do weathering rates differ in the laboratory and field? *Chemical Geology* **202**(3–4): 479–506.

White AF, Schulz MS, Blum AE, Huntington TG, Peters NE. 2001. Differential rates of feldspar weathering in granitic regoliths. *Geochimica et Cosmochimica Acta* **65**(6): 847–869.

Yoo K, Amundson R, Heimsath AM, Dietrich WE. 2006. Spatial patterns of soil organic carbon on hillslopes: integrating geomogrphic processes and the biological C cycle. *Geoderma* **130**(1–2): 47–65.

Yoo K, Amundson R, Heimsath AM, Dietrich WE, Brimhall GH. 2007. Integration of geochemical mass balance with sediment transport to calculate rates of soil chemical weathering and transport on hillslopes. *Journal of Geophysical Research* **112**: F02013: 1–15. DOI: 10.1029/2005JF000402